

ABSTRACT

BODDA, SARAN SRIKANTH. Multi-Hazard Risk Assessment of a Flood Defense Structure. (Under the direction of Dr. Abhinav Gupta).

Safety of nuclear plants against external events has gained significant attention in the last decade. Fukushima Daiichi nuclear power station disaster occurred due to flooding of the plant which was caused by the Great East Japan earthquake and subsequent tsunami. In the US, Oyster Creek nuclear plant was shut down when high storm surge during hurricane Sandy threatened its water intake and circulation systems. These nuclear facilities can be protected from floods through the use of flood protection systems such as floodwalls, dams, and weirs. A flood defense structure located upstream of a power plant can undergo seismic failure or flooding failure leading to flooding at the nuclear plant. Flooding initiated by collapse of the dam can cause failure at the nuclear power plant due to loss of power supply, loss of cooling, loss of reactors, and release of radiation. All the flood defense structures are subjected to scour around their foundations. The stability of the foundation is endangered when the scour depth becomes significant at the downstream toe. This research explores the effect of scouring on the fragility of a concrete weir structure. It also evaluates the fragilities for failure of a concrete floodwall due to various failure modes under a multi-hazard scenario (flooding and seismic events). Structural failure of concrete floodwall is characterized by excessive deformation failure mode for seismic loads. The failure modes considered for flooding loads are rigid body failure and foundation failure.

© Copyright 2018 by Saran Srikanth Bodda

All Rights Reserved

Multi-Hazard Risk Assessment of a Flood Defense Structure

by
Saran Srikanth Bodda

A thesis submitted to the Graduate Faculty of
North Carolina State University
in partial fulfillment of the
requirements for the Degree of
Master of Science

Civil Engineering

Raleigh, North Carolina

2018

APPROVED BY:

Dr. M. Shamim Rahman

Dr. Gnanamanikam Mahinthakumar

Dr. Abhinav Gupta
Chair of Advisory Committee

DEDICATION

To My Parents

BIOGRAPHY

Saran Srikanth Bodda was born and brought up in the city of Vizag in India. He joined the undergraduate program in Civil Engineering at Indian Institute of Technology, Guwahati, India in 2010 and received the Bachelors of Technology degree in July, 2014. He joined North Carolina State University in Spring 2015 to pursue his Master of Science in Civil Engineering and is currently working towards obtaining PhD degree.

Saran is a member of Tau Beta Pi at NC State University. He also got an internship opportunity at Idaho National Laboratory in Summer 2017. Apart from research, he has served as a Teaching Assistant for both undergraduate and graduate courses in Structural Engineering and Mechanics in NC State University. Saran's research interests include structural dynamics, probabilistic risk assessment, scientific computing, earthquake engineering, Bayesian statistics and Bayesian network.

ACKNOWLEDGEMENTS

Firstly, I would like to express my sincere gratitude to my advisor, Dr. Abhinav Gupta, for giving me the opportunity to pursue my graduate studies at NCSU. His patience, motivation, immense knowledge and constant guidance helped me during the entire research work and in writing this thesis. I would also like to thank Dr. Shamim Rahman and Dr. Kumar Mahinthakumar for graciously agreeing to serve on my advisory committee and for their valuable suggestions.

I am grateful to my undergrad advisor, Dr. Hrishikesh Sharma, for enlightening me the first glance of research. A very special thanks to Akshay Reddy and Satyavati, for giving me inspiration and motivation to pursue research. I thank my colleagues and friends – Harleen, Payel, Shinyoung, Ankit Dubey, Sugandha, Krishna Chaitanya and Uday Teja for their useful insights, feedback, and precious support without which it would not be possible to conduct this research.

I express a profound gratitude to my parents and to my brother for providing me with constant support and continuous encouragement throughout my life in general and through the process of writing this thesis. This accomplishment would not have been possible without them.

Finally, the research was supported by the Center for Nuclear Energy Facilities and Structures (CNEFS) at North Carolina State University. I am greatly indebted to the center for providing me with all the facilities and support throughout my graduate school. I would also like to thank all the staff members of the Civil Engineering department for their help and support extended over the years.

TABLE OF CONTENTS

LIST OF TABLES	viii
LIST OF FIGURES	ix
PART I: INTRODUCTION.....	1
1. General	2
2. Literature Review	3
3. Objective.....	4
4. Organization	5
REFERENCES	6
PART II: FRAGILITY OF A WEIR STRUCTURE DUE TO SCOURING.....	9
1. Introduction	10
2. Problem Description.....	12
2.1 Description of the Weir Structure	12
2.2 Steady-State Seepage formulation	13
2.3 Performance Criterion.....	15
3. Finite Element Modeling.....	17
3.1 Efficiency	17
3.2 Numerical Instability.....	19
3.3 Convergence and Accuracy.....	21
4. Effect of Soil Anisotropy on Exit Gradient.....	24

5. Effect of Scouring on Exit Gradient	25
6. Flooding Fragility Analysis	30
7. Conclusions	33
REFERENCES	35
PART III: MULTI-HAZARD FRAGILITY ASSESSMENT OF A CONCRETE FLOODWALL.....	38
1. Introduction	39
2. Problem Description.....	41
3. Flooding Fragility Analysis.....	41
3.1 Failure in Stability.....	41
3.2 Failure in Instability	50
3.3 System Level Flooding Fragility.....	54
4. Seismic Fragility Analysis.....	55
4.1 Fluid Structure Interaction (FSI) Formulation	55
4.2 Modeling of Floodwall and Reservoir System.....	59
4.3 Time History Analysis of Reservoir-Floodwall System	60
4.4 Seismic Fragility Surface	63
5. Multi-hazard Fragility Assessment.....	66
6. Conclusions	67
REFERENCES	69

PART IV: SUMMARY AND CONCLUSIONS.....	72
1. Summary.....	73
2. Conclusions	73
3. Recommendations for Future Research.....	74

LIST OF TABLES

PART II: FRAGILITY OF A WEIR STRUCTURE DUE TO SCOURING

Table 1. Minimum critical gradient for sand, silt, and clay soils	16
Table 2. Results of convergence study using 4-noded elements.....	18
Table 3. Results of convergence study using 6-noded elements.....	18
Table 4. Results of convergence study using 8-noded elements.....	19
Table 5. Convergence study for calculating the upstream width	23
Table 6. Convergence study for calculating the downstream width	23
Table 7. Convergence study for calculating the Depth of the soil domain	24
Table 8. Effect of Soil Anisotropy on Exit Gradient.....	25
Table 9. Results of convergence study using 4-noded elements.....	27
Table 10. Results of convergence study using 6-noded elements.....	27
Table 11. Results of convergence study using 8-noded elements.....	28
Table 12. Effect of Downstream water level on Maximum Exit Gradient	29
Table 13. Maximum Exit Gradient for different scour profiles	29

PART III: MULTI-HAZARD FRAGILITY ASSESSMENT OF A CONCRETE

FLOODWALL

Table 1. Random variables and deterministic values used to evaluate fragility curves	48
Table 2. Random variables and deterministic values used to evaluate fragility curves	53
Table 3. Selected ground motions	64

LIST OF FIGURES

PART II: FRAGILITY OF A WEIR STRUCTURE DUE TO SCOURING

Fig. 1. Geometry and Dimensions (m) of the Weir structure foundation	13
Fig. 2. Fluid flow in two directions	14
Fig. 3. Vector plot of hydraulic gradient using 8-noded element of size $h =$ $2 m$	21
Fig. 4. Vector plot of hydraulic gradient using 8-noded element of size $h =$ $0.5 m$	21
Fig. 5. Dimensions of the scour at the toe of the stilling basin.....	26
Fig. 6. Distributions of the random variables used to evaluate fragility curves	31
Fig. 7. Fragility curves for rupture failure for fixed $Ds = 1.5 m$ and varying $Bs = 2, 3, 4 m$	32
Fig. 8. Fragility curves for rupture failure for fixed $Bs = 3 m$ and varying $Ds =$ $1, 1.5, 2 m$	33

PART III: MULTI-HAZARD FRAGILITY ASSESSMENT OF A CONCRETE FLOODWALL

Fig. 1. Loads acting on the floodwall	42
Fig. 2. Failure by sliding, overturning, and compression failure of foundation (FEMA259, 2012).....	47
Fig. 3. Fragility curve due to sliding failure	49
Fig. 4. Fragility curve due to compression failure of foundation at toe	49
Fig. 5. Boundary conditions for the seepage analysis	51

Fig. 6. Fragility curve due to rupture failure	53
Fig. 7. System level flooding fragility curve	54
Fig. 8. Boundary conditions of the fluid domain.....	56
Fig. 9. Finite element model of floodwall reservoir system.....	60
Fig. 10. Acceleration Time History of Oroville earthquake scaled to 0.1g PGA.....	61
Fig. 11. Horizontal displacement time history at the wall crest with full reservoir	62
Fig. 12. Hydrodynamic Pressure envelope acting on the upstream face of the floodwall	62
Fig. 13. Response spectral acceleration of selected ground motions	65
Fig. 14. Fragility curve due to excessive deformation failure mode for a flood level of 2.5 m	65
Fig. 15. Seismic fragility surface due to excessive deformation failure mode.....	66
Fig. 16. Multi-hazard fragility surface.....	67

PART I: INTRODUCTION

1. General

In recent years, flooding at critical facilities has highlighted the significance of maintaining the performance levels of its flood defense systems. In the US, the South Texas Project nuclear plant (Queally, 2017) was shut down when heavy floods during hurricane Harvey threatened an embankment dam that surrounds the nuclear plant. Many nuclear plants (Salem, Nine Mile Point, Indian Point, and Oyster Creek) were shut down due to flooding from hurricane Sandy (Mufson, 2012). These facilities are typically located near a body of water such as a river, lake, an estuary or sea because they require abundant and dependable source of water supply. External flood protection systems such as floodwalls or weir structures are often constructed to prevent flooding at such critical facilities.

When a flood defense structure fails, it can cause flooding at the facility which can be catastrophic. The risk of flooding at a site is directly related to the fragility of a flood defense structure located upstream of the critical facility. Some of the nuclear power plants (NPP) with upstream dams are Arkansas NPP, Three Mile Island, and Fort Calhoun Nuclear Station (Perkins, 2011). In rare cases, seismically induced failure of flood defense structures would result in flooding at the facility. Therefore, it is essential to evaluate the risk of flood protection systems under multi-hazard scenario for developing the flooding probabilistic risk assessment (PRA) for nuclear power plants. The scope of this study is to obtain the fragility of a flood defense structure due to flooding and seismic events by accounting for various critical failure modes. These failure modes are adequately expressed to represent the failure through the use of performance functions.

2. Literature Review

Many studies (Kaida and Miyagawa, 2016; Sandhu, 2015; Mouyeaux et al., 2015; Ju and Jung, 2015; Schweckendiek and Calle, 2013; Lupoi and Callari, 2012; Rajabalinejad et al., 2007; Tekie and Ellingwood, 2002; Ellingwood and Tekie, 2001) have presented the fragility curves for failure of flood defense structures, such as concrete dams, floodwalls, weir structures, embankment dams, and levees.

Sandhu (2015) defines various limit states and a set of random variables affecting the concrete gravity dam's performance to conduct the probabilistic safety assessment (PSA) of the dam for the flooding hazard. Ju and Jung (2015) conduct seismic probabilistic risk assessment and its application to the case of the Gangjeong-Goryeong weir in Korea. Schweckendiek and Calle (2013) develop the flooding fragility curves for the piping foundation failure of a levee. Lupoi (2012) presents a methodology to conduct a system level seismic fragility analysis of the Kasho dam. However, none of these studies consider: (a) the effect of scouring on the foundation failure due to rupture in their research (b) PSA study of a concrete flood defense structure considering a comprehensive set of failure modes particularly under a multi-hazard scenario.

The probabilities of failure for foundation failure due to rupture is obtained from a seepage analysis. Several studies (Broaddus, 2015; Kirra, 2015; Sandhu, 2015; Kolawole, 2013; Hasani, 2013; Soleymani, 2011; Noori, 2011; Saleh, 2009) have been conducted in the past to evaluate seepage through the flood defense structure or under its foundation using finite element method. Most of these studies (Broaddus, 2015; Kirra, 2015; Sandhu, 2015; Kolawole, 2013; Noori, 2011; Saleh, 2009) have used 4-noded quadratic elements to model the seepage problem. However, using 4-noded elements for a scour profile can be computationally

inefficient for a probabilistic study and can also cause numerical instability if the element size is inappropriate. The dimensions of various flood defense structures considered for the seepage analysis are mentioned in previous studies (Broaddus, 2015; Hasani, 2013; Soleymani, 2011; Saleh, 2009), but none of these studies have given any guidance on the size of the elastic half space. If the size of the elastic half space is less than an optimal size, elastic half space can make a significant difference in the exit gradient calculation.

3. Objective

A study of the past research illustrates that the flood defense structures have not been evaluated for the foundation failure due to the effect of scouring. Also, there are no existing studies on evaluating the fragilities of a flood defense structure considering a set of failure modes under a multi-hazard scenario. In the present study, the effect of scouring on the foundation failure is demonstrated for a concrete weir structure. Multi-hazard fragility assessment is illustrated for a concrete floodwall. The key steps undertaken to conduct this research are:

- Develop a finite element model for rupture analysis of the weir structure that is computationally efficient and accurate.
- Conduct a probabilistic study of the weir structure by considering uncertainties in the random variables that characterizes the performance function to obtain the fragility curve. Consider different scour profiles to study its variation in fragility curves.
- Identify the failure modes of the concrete floodwall for the flooding and the seismic events.

- Define the performance functions for the failure modes and include the uncertainties in material properties, foundation soil, earthquake and flooding loads.
- Conduct seismic analysis and seepage analysis of the floodwall using finite element methods.
- Conduct a multi-hazard fragility assessment of the concrete floodwall due to combined flooding and seismic events.

4. Organization

This thesis primarily consists of four parts. Part-I gives an introduction to the problem being studied followed by a discussion of the objective of the research. In the second part, the effect of scouring on the flooding fragility of a concrete weir structure is evaluated. Challenges associated with efficiency and accuracy of the finite element seepage model are also presented. The third part includes probabilistic safety assessment (PSA) of a concrete floodwall considering various failure modes under a multi-hazard scenario. A multi-hazard fragility surface due to combined seismic and flooding events is presented.

Finally, fourth part presents a summary and conclusions of the work that has been discussed in Part-II and Part-III. It also proposes recommendations for future work.

REFERENCES

- Broaddus, M. R. (2015). "Performing a steady-state seepage analysis using SEEP/W : a primer for engineering students," Electronic Theses and Dissertations. Paper 2219.
- Ellingwood, B., and Tekie, P. B. (2001). "Fragility analysis of concrete gravity dams," *Journal of infrastructure systems*, 7(2), 41-48.
- Hasani, H., Mamizadeh, J., and Karimi, H. (2013). "Stability of Slope and Seepage Analysis in Earth Fills Dams Using Numerical Models (Case Study : Ilam Dam- Iran)," *World Applied Sciences Journal*, 21(9).
- Ju, B. S., and Jung, W. (2015). "Evaluation of Seismic Fragility of Weir Structures in South Korea," *Mathematical Problems in Engineering*, 10 pages.
- Kaida, H., Miyagawa, Y., and Kihara, N. (2016). "Methodology for Fragility Evaluation of a Seawall Against Tsunami Effects," ASME, International Conference on Nuclear Engineering.
- Kirra, M. S., Zeidan, B. A., Shahien, M. M., and El-Shemy, M. (2015). "Seepage Analysis of Walter F. George Dam, USA: A case Study," *International Conference on Advances in Structural and Geotechnical Engineering*, 6-9 April 2015, Hurgada, Egypt.
- Kolawole, A. O. and Oluwole A. A. (2013). "A Study of Seepage through Oba Dam Using Finite Element Method," *Civil and Environmental Research*, 3, 3 (ISSN 2222-1719).
- Lupoi, A. and Callari, C. (2011). "A probabilistic method for the seismic assessment of existing concrete gravity dams," *Structure and Infrastructure Engineering*, 8(10), 985-998.

- Mouyeaux, A., Carvajal, C., Peyras, L., Bressolette, P., Breul, P., and Bacconnet, C. (2015). "Probability of failure of an embankment dam due to slope instability and overtopping," 13th ICOLD Benchmark Workshop on Numerical Analysis of Dams, Lausanne.
- Mufson, S. (2012). "3 nuclear power reactors shut down during Hurricane Sandy," *The Washington Post*.
- Noori, B. A. and Ismaeel, K. S. (2011). "EVALUATION OF SEEPAGE AND STABILITY OF DUHOK DAM," *Al-Rafadain Engineering Journal*, 19(1), 42-58.
- Queally, J. (2017). "As Historic Flooding Grips Texas, Groups Demand Nuclear Plant Be Shut Down," *CommonDreams*.
- Sandhu, H. K. (2015). "Flooding Fragility of Concrete Gravity Dam-Foundation System," Master of Science Thesis, Department of Civil Engineering, North Carolina State University, Raleigh, NC.
- Saleh, I. K., Aqeel, S. A., and Rafid, and S. R. (2009). "Seepage Analysis underneath Diyala Weir Foundation," *Thirteenth International Water Technology Conference, IWTC 13 2009*, Hurghada, Egypt.
- Schweckendiek, T., and Calle, E. O. F. (2013). "Updating levee reliability with performance observations," *Conversion of Large Scale Wastes into Value-added Products*, 87.
- Soleymani, S. and Akhtarpur, A. (2011). "Seepage Analysis for Shurijeh Reservoir Dam Using Finite Element Method," *Geo-Frontiers Congress*, American society of civil engineering.

Tekie, P. B. and Ellingwood, B. R. (2003). "Seismic fragility assessment of concrete gravity dams," *Earthquake Engineering and Structural Dynamics*, 32(14), 2221-2240.

PART II: FRAGILITY OF A WEIR STRUCTURE DUE TO SCOURING

1. Introduction

In recent years, several catastrophic flooding accidents have occurred at critical facilities. The Arkema chemical plant in Texas suffered chemical explosion because hurricane Harvey related flooding resulted in a loss of power supply (CNBC, 2017). Fukushima Daiichi nuclear disaster (IAEA, 2015) occurred due to loss of external and backup power supplies following the tsunami induced flooding. In order to prevent flooding at such critical and toxic facilities, flood protection systems such as floodwalls or weir structures are being planned or have been constructed.

The risk of flooding at critical facilities which are located on the downstream side of a flood defense structure is directly related to the fragility of flood defense structure. According to FEMA (2017), 20 dams were breached due to foundation failures, flood overflow, and concrete cracks as a result of flooding due to Hurricane Matthew in North Carolina. Flooding produced by Hurricane Katrina breached many levees which resulted in flooding of approximately 75% of the New Orleans metropolitan area (Robert, 2006).

The data for generating the flooding fragility curves for foundation failure is obtained from a seepage analysis. Therefore, the reliability of the fragility curves largely depends on accuracy of the seepage model. Various methods such as flow nets, experimental and numerical methods (finite difference and finite elements) have been used in the past to solve the two dimensional partial differential equation for seepage flow (USACE, 1993; Billstein, 1999; Saleh, 2009; Kolawole, 2013; Kirra, 2015; Sandhu, 2015). USACE (1993) uses graphical flow nets for estimating seepage through embankments and foundations. Numerical modeling has been used successfully to solve seepage problems (Naouss, 1995). Billstein et al. (1999) use numerical, analytical and experimental models to determine the seepage levels

and discharge. Saleh (2009) uses FE modeling to analyze seepage flow under weir foundation. Kolawole (2013) and Kirra et al. (2015) use FE modeling to study seepage through earth dams. Bardet (2002) uses finite difference methods for solving free surface seepage problems. Finite element method is widely preferred because of its ability to handle complex geometries (and boundaries) with relative ease.

Flood defense structures are subjected to scour around their foundations. If the scour depth becomes significant, the foundation of the structure is exposed, with a consequent risk of rupture failure. Therefore, it is important to study the effect of scour on foundation failure. Failures of Woodlake dam (FEMA, 2017) and Hope Mills dam (ABC11, 2010) occurred primarily due to scouring. While several studies have been conducted in the past to evaluate the effect of seepage (Saleh, 2009; Kolawole, 2013; Kirra, 2015; Sandhu, 2014; Broaddus, 2015), none of these studies consider the effect of scouring, which is typically the primary initiator of the foundation failure. In this paper, we present the results of a study that evaluates the effect of scouring on the fragility of concrete weir structure. Given the uncertainties in the soil properties as well as the potential erosion profiles, a probabilistic study is conducted by considering uncertainties in relevant properties to evaluate the fragility curves (probabilities of failure). Variation in these curves due to a change in scour profile is also presented. To begin with, a finite element based approach appeared to be straightforward for conducting this study. However, it exhibited challenges associated with computational efficiency, numerical stability, and accuracy. These challenges and the solutions to overcome them are also presented in this paper.

2. Problem Description

As mentioned above, a primary reason for failure of flood defense structures is related to seepage through the soil which has the potential to cause internal erosion and scouring on the downstream of the structure. Even at low hydraulic heads, the flow over a structure such as weir has a significant potential for scour. Hence, stilling basins are placed at the ends of weir spillways to dissipate the energy of water exiting the spillway and mitigate scouring. However, local scour downstream of stilling basins is considered as an important phenomenon as it can endanger the stability of the foundation with a consequent risk of failure when the scour depth becomes significant (Elnikhely, 2017). The study presented in this research is carried out for a simple model of weir structure. However, the concepts are directly applicable to any concrete flood defense structure.

2.1 Description of the Weir Structure

Geometry and dimensions of the particular section of a weir structure foundation considered for this study are shown in Fig. 1 (Ju and Jung, 2015). Potential head on upstream is $H_{u/s} = 11\text{ m}$. The soil foundation at the site consists of silty sand. A part of the weir's concrete structure is built into the foundation with a depth of 10 m. To begin with, the width (B) and depth (D) of the elastic half space are assumed to be $B = 80\text{ m}$ and $D = 50\text{ m}$ respectively. These dimensions are consistent with the values considered in many prior studies. B_1 and B_2 are the widths of the soil domain on upstream side and downstream side of the weir structure, respectively.

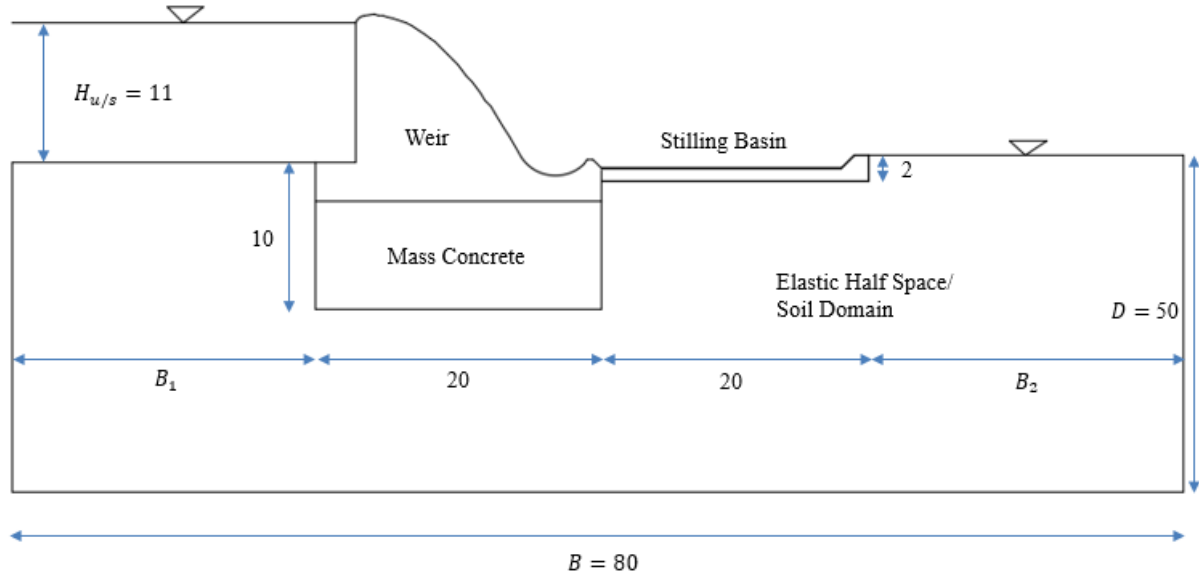


Fig. 1. Geometry and Dimensions (m) of the Weir structure foundation

2.2 Steady-State Seepage formulation

All flood defense structures have some seepage (flow of water through soils) as there is difference in water pressure between upstream and downstream side of the defense structure. Seepage of water through foundation depends on several factors, including the soil permeability, hydraulic gradient, and type of flow. Higher water levels in the reservoir result in higher gradient for seepage through the foundation and thereby increasing the subsequent chances of a foundation failure. Uncontrolled seepage can slowly erode soil from flood defense structure's foundation. Erosion of the soil starts at the downstream side of the flood defense structure and advances progressively toward the reservoir, creating a hollow pipe like formation to the reservoir, leading to foundation failure and hence, collapse of the structure. This phenomenon is known as piping or undermining.

The two-dimensional steady-state flow of the pore fluid is governed by Laplace's equation, as shown in Eq. (1):

$$K_x \frac{d^2 H}{dx^2} + K_y \frac{d^2 H}{dy^2} = 0 \quad (1)$$

where: K_x and K_y are the hydraulic conductivity in the x and y directions respectively and H is the hydraulic head.

The seepage flow q_x and q_y in the x and y directions respectively is calculated from Darcy's law as shown in Eq. (2). These flow quantities are directed either in the x direction or in the y direction. The total flow at any point in the foundation is the resultant of the q_x and q_y at that point. Thus the total seepage-flow vector is directed so that it is perpendicular to the lines of constant head (equipotential lines) in the foundation, as shown in Fig. 2.

$$\begin{aligned} q_x &= -K_x \frac{\partial H}{\partial x} \\ q_y &= -K_y \frac{\partial H}{\partial y} \end{aligned} \quad (2)$$

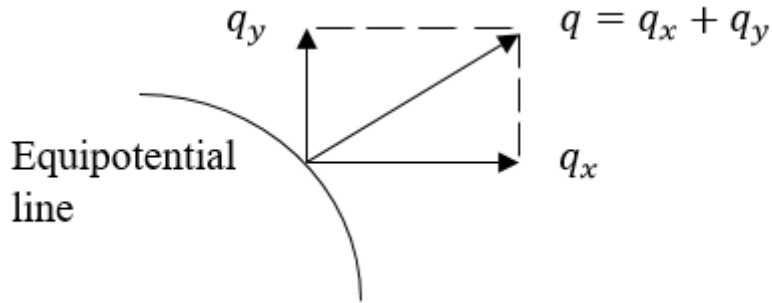


Fig. 2. Fluid flow in two directions

The Galerkin's discretization of the Laplace equation gives the following relation:

$$[K]\{H\} = \{Q\} \quad (3)$$

where: $[K]$ is the global stiffness matrix, $\{H\}$ is an unknown nodal total head vector, and $\{Q\}$ is a nodal flow vector.

The global stiffness matrix $[K]$ is an assembly of the element stiffness matrices of the entire flow domain. The element stiffness matrix is given as:

$$[K] = \int_{v_e} [B]^T [k] [B] dv \quad (4)$$

where: v_e is the domain of the element, $[B]$ is derived from the shape function $[N]$, and $[k]$ is the element permeability matrix, defined as

$$[k] = \begin{bmatrix} K_x & 0 \\ 0 & K_y \end{bmatrix} \quad (5)$$

In this study, the seepage equation is solved using FE method based on the approach by Kratochvil (2004) and Kirra (2015).

2.3 Performance Criterion

A fragility assessment requires characterization of failure in terms of a performance function. The performance function defines the governing limit-state to evaluate the probabilities of failure. In this study, the performance function characterizes failure as a rupture of the foundation. Rupture of the foundation occurs when maximum exit gradient exceeds the critical gradient. The exit gradient (i_{ex}) is the total head loss divided by distance of flow between the two measured head locations, calculated at the downstream area where seepage exits the porous media. The area of significance in this study is along the downstream edge of weir structure for confined flow. The exit gradient is calculated along the downstream side, and maximum gradient usually occurs near the toe of the stilling basin. Also, for a two-

dimensional model, the exit gradient depends upon the gradient direction. The critical gradient (i_{cr}) is based on the foundation soil properties.

$$i_{cr} = (G_s - 1)(1 - n) \quad (6)$$

$$i_{ex} = \frac{dH}{dL} \quad (7)$$

where: n is the porosity of the soil, and G_s is the specific gravity of the soil.

The performance function for rupture is characterized by following limit state:

$$Z_r = i_{cr} - i_{ex} \quad (8)$$

And the conditional probability of rupture failure given flood height is expressed as:

$$P_f(\text{rupture}|\text{flood height}) = P(Z_r < 0) \quad (9)$$

For the worst case scenario of the rupture to occur, minimum value of specific gravity and maximum value of porosity are chosen from various ranges of soil specific gravity and porosity so that the hydraulic critical gradient is minimum (Sandhu, 2015). The minimum critical gradient calculated for three different types of soils is shown in Table. 1.

Table 1. Minimum critical gradient for sand, silt, and clay soils

	Soil Type	Specific Gravity	Porosity (%)	Minimum Critical Gradient (i_{cr})
1	Sand	2.63	53	0.7661
2	Silt	2.65	61	0.6435
3	Clay	2.70	57	0.7310

3. Finite Element Modeling

3.1 Efficiency

A probabilistic study to evaluate fragilities requires a large number of finite element analyses. Therefore, computational efficiency is an important consideration. The type and the size of specific elements used for creating the model can have a significant impact on both the efficiency as well as accuracy. In most of the prior studies (Saleh, 2009; Noori, 2011; Kolawole, 2013; Kirra, 2015; Broaddus, 2015), 4-noded quadratic elements are used to model the seepage problem. In this study, we observe that this element type requires a very fine mesh in order to accurately model the scour profile which in turn makes the analysis computationally inefficient. Therefore, alternative element types are explored. Two types of alternatives considered include the use of a 6-noded triangular element and an 8-noded quadratic element. These two element types are chosen because of their ability to represent curved scour profiles accurately through a relatively coarser mesh. In order to compare the efficiency and accuracy of these different element types, a simpler case with no scouring is considered. The effect of scouring is studied after a particular element type is selected.

The two-dimensional finite element idealization of the foundation consists of uniform elements with an element size of ' h ' meters in both the horizontal and vertical directions. The soil layer is assumed to be homogenous and isotropic with respect to permeability. Tables 2 – 4 present the results of the convergence (accuracy) as well as computational efficiency conducted for the 3 types of elements considered. Computation time ' t ' is taken as the unit time equal to the run time of the FE model with 4-noded elements of an element size $h = 2\text{ m}$. The computation time for other mesh sizes and elements are expressed as a multiple of t .

Table 2. Results of convergence study using 4-noded elements

Mesh	Element Size, <i>h</i> (m)	Computing Time	Maximum Exit Gradient	Relative Error
1	2	t	0.4804	
2	1	$2t$	0.3963	17.51 %
3	0.5	$9.21t$	0.3895	1.72 %
4	0.25	$62.1t$	0.3860	0.90 %
5	0.125	$362t$	0.3848	0.31 %

Table 3. Results of convergence study using 6-noded elements

Mesh	Element Size, <i>h</i> (m)	Computing Time	Maximum Exit Gradient	Relative Error
1	2	t	0.3988	
2	1	$2t$	0.3866	3.07 %
3	0.5	$7.02t$	0.3851	0.39 %
4	0.25	$27.1t$	0.3845	0.16 %
5	0.125	$126t$	0.3842	0.08 %

Table 4. Results of convergence study using 8-noded elements

Mesh	Element Size, h (m)	Computing Time	Maximum Exit Gradient	Relative Error
1	2	t	0.3634	
2	1	$2t$	0.3807	4.76 %
3	0.5	$10t$	0.3845	1.01 %
4	0.25	$45.1t$	0.3844	0.03 %
5	0.125	$234t$	0.3842	0.05 %

According to the convergence analysis, quadratic elements (8-noded and 6-noded) exhibits much smaller error than linear elements (4-noded) for the same element size, which is expected due to richer interpolation in 8-noded and 6-noded elements. Based on optimal combination of accuracy and efficiency, the FE model with 8-noded elements of $h = 0.5$ m is chosen for the further analysis.

3.2 Numerical Instability

A seepage analysis provides information of flow magnitude and the direction of flow in different regions of the foundation. Such a spatial mapping of the flow is represented in terms of hydraulic gradient vectors. Selection of element size not only influences convergence and computational efficiency as discussed in previous section, it can also cause numerical instability particularly in the evaluation of hydraulic exit gradient. To illustrate this, let us consider the plot of gradient vectors shown in Fig. 3. The gradient vectors in this figure are evaluated for the case of an element size $h = 2$ m and the point B represents the toe, i.e. the

thickness of stilling basis is equal to the element size. It can be observed that the maximum exit gradient occurs at surface of the toe of stilling basin. In this particular case, the exit gradient is calculated based on Eq. (10), in which the hydraulic head at point B is also the hydraulic head at toe ($H_B = H_{toe}$).

$$i_{ex} = \frac{H_A - H_B}{L_{AB}} \quad (10)$$

However, the toe is a sharp reentrant corner which is a point of discontinuity in the foundation profile. The discontinuity would therefore result in a singularity, i.e. the derivatives of the dependent variables for partial differential equation (Eq. 1) do not exist at the sharp toe thereby resulting in a numerical instability.

A smaller element size allows more than one element to span across the thickness of the stilling basis and the point B moves away from the toe. For example, in case of $h = 0.5 \text{ m}$, the exit gradient is not influenced by the sharp corner at the toe. The gradient vectors near the toe of the stilling basin for $h = 0.5 \text{ m}$ are shown in Fig. 4.

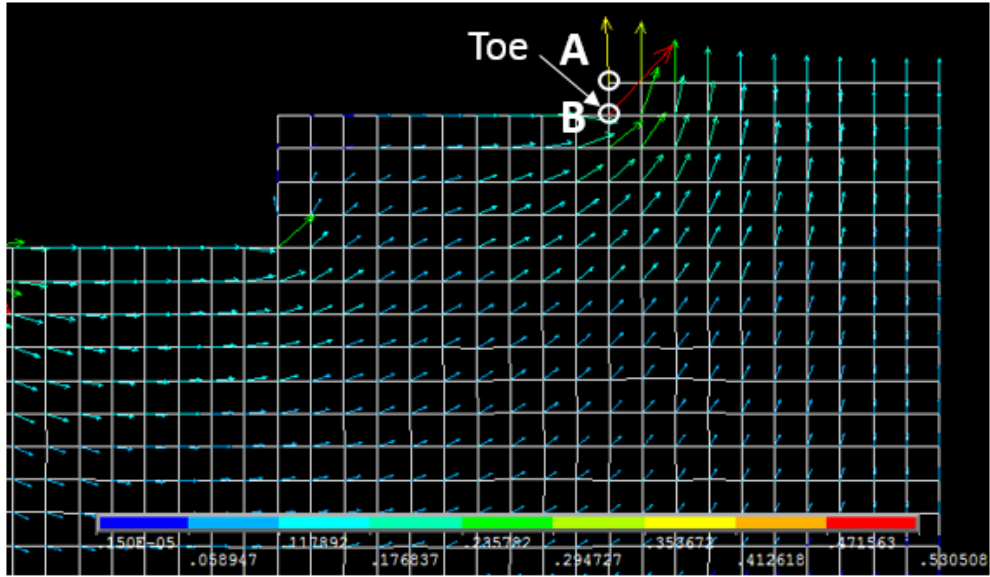


Fig. 3. Vector plot of hydraulic gradient using 8-noded element of size $h = 2\text{ m}$

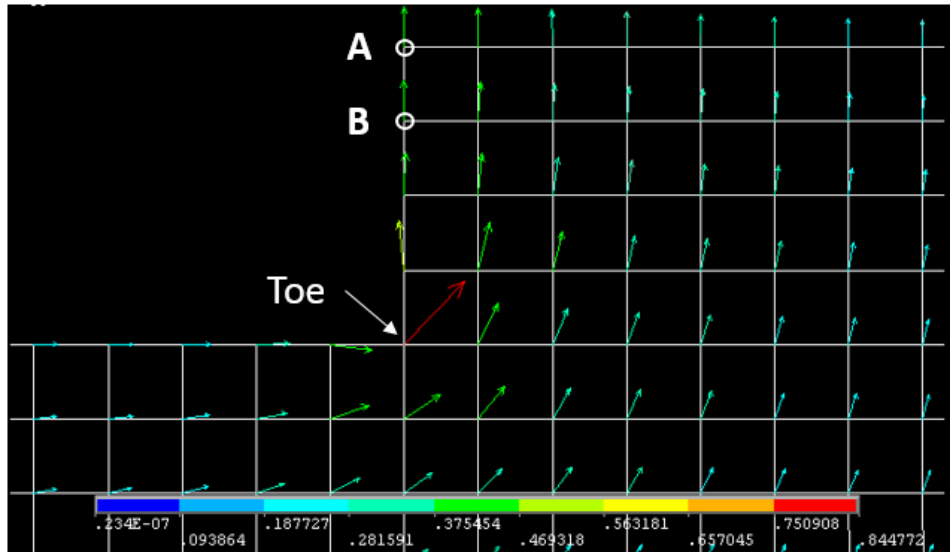


Fig. 4. Vector plot of hydraulic gradient using 8-noded element of size $h = 0.5\text{ m}$

3.3 Convergence and Accuracy

In general, the soil domain is considered as a semi-infinite or an elastic half space, i.e. a finite soil domain is modelled such that there is no effect of limited domain on the exit

gradient. The dimensions of various flood defense structures considered for the seepage analysis are mentioned in previous studies (Saleh, 2009; Soleymani, 2011; Hasani, 2013; Broaddus, 2015), but none of these studies have given any guidance on the size of the elastic half space. The size of the elastic half space can make a significant difference in exit gradient calculation as seen in Tables 5 – 7. If the upstream width and depth of the soil domain is less than an optimal size, then the results are underestimated and if the downstream width of the soil domain is less than an optimal size, then the results are overestimated.

The optimal dimensions of the soil domain are assessed through a convergence study on maximum exit gradient. This study comprised of following three steps. Step 1: The upstream (U/S) width is calculated by fixing both the downstream (D/S) width and depth of the soil domain as shown in Table. 4. Step 2: The D/S width is calculated by fixing the depth of the soil domain, and the U/S width obtained from step 1 as shown in Table. 5. Step 3: The depth of the soil domain is calculated by fixing the U/S and D/S widths obtained from step 1 and step 2 as shown in Table. 6.

It is observed that the upstream width (B_1), the downstream width (B_2), and the depth (D) of the elastic half space should be at least two and half times more than the combined width of the weir structure and the stilling basin.

Table 5. Convergence study for calculating the upstream width

	Upstream Width (B_1)	Maximum Exit Gradient	Relative Error
D/S width ($B_2 = 20\text{ m}$)	10	0.3089	
	20	0.3845	24.47 %
Depth ($D = 50\text{ m}$)	40	0.4346	13.03 %
	60	0.4475	2.97 %
	80	0.4511	0.80 %
	100	0.4521	0.22 %

Table 6. Convergence study for calculating the downstream width

	Downstream Width (B_2)	Maximum Exit Gradient	Relative Error
U/S width ($B_1 = 100\text{ m}$)	10	0.5779	
	20	0.4521	21.77 %
Depth ($D = 50\text{ m}$)	40	0.3783	16.32 %
	60	0.3593	5.02 %
	80	0.3540	1.48 %
	100	0.3525	0.42 %

Table 7. Convergence study for calculating the Depth of the soil domain

	Depth (D)	Maximum Exit Gradient	Relative Error
U/S width ($B_1 = 100\text{ m}$)	20	0.2530	
	40	0.3389	33.95 %
D/S width ($B_2 = 100\text{ m}$)	60	0.3606	6.40 %
	80	0.3691	2.36 %
	100	0.3738	1.27 %
	120	0.3765	0.72 %

The convergence study for the elastic half space was also carried out for various other combinations of B_1 , B_2 and D as well (e.g. B_1 is calculated by fixing $B_2 = 100\text{ m}$ and $D = 120\text{ m}$). Although, the results are not presented here for brevity, same results were observed.

4. Effect of Soil Anisotropy on Exit Gradient

Although the elastic half space is considered to be homogenous in the preliminary study discussed above, most of the soils are anisotropic in nature. Anisotropy depends upon the soil properties which defines the preferential flow direction in soils. Usually, in the compaction process, the soil is laid in horizontal layers and then compacted, therefore the tendency of flow is maximum in the horizontal direction. Anisotropy ratio relates the coefficient of permeability in different directions and is defined as the ratio of vertical to horizontal hydraulic conductivity (K_y/K_x). Anisotropy ratio of compacted soils typically varies between 0.025 to 1 (Sommai, 1992). Table 8 shows the effect of anisotropy on exit gradient. With the decrease in anisotropic

ratio, the exit gradient increases. The analysis is carried out using 8-noded elements of an element size $h = 0.5 \text{ m}$.

Table 8. Effect of Soil Anisotropy on Exit Gradient

K_y/K_x	Maximum Exit Gradient
0.025	0.5409
0.1	0.4965
0.25	0.4631
0.5	0.4295
1	0.3845
2	0.3285

5. Effect of Scouring on Exit Gradient

The profile of a local scour is difficult to estimate due to the complexity of scour dynamics. Many experimental studies using laboratory tests have been performed in the past for predicting the depth, length, and shape of scour profile and its temporal growth. Oliveto et al. (2010) investigated time-dependent and spatial evolution of local scour downstream below low-head spillways followed by stilling basins. Dehghani et al. (2010) evaluated local scour characteristics downstream of rectangular sharp-crested weirs. In this research, the geometry of the scour profile is chosen in accordance with the existing studies (Oliveto et al., 2010; Dehghani et. al, 2010; Farhoudi and Shayan, 2014).

For the weir structure foundation with scouring, the convergence analysis is carried out for two different types of mesh refinement (a). Uniform mesh refinement (b). Adaptive mesh

refinement (AMR). For simple geometries, a grid of uniform mesh spacing gives satisfactory results. However, for geometries that exhibit steep gradients or discontinuities, uniform mesh with very fine spacing can be used to minimize the estimated local error. But this approach can be computationally inefficient. Therefore, AMR is used in this study.

The scour starts at the toe of the stilling basin as shown in Fig. 5, where B_s is the width and D_s is the depth of the scour. In this analysis, homogenous soil layer with isotropic permeability is considered and the scour profile is assumed to be $B_s = 5\text{ m}$, $D_s = 2\text{ m}$. The results of computational accuracy and convergence conducted for 4-noded, 6-noded, and 8-noded elements are presented in Tables 9 – 11.

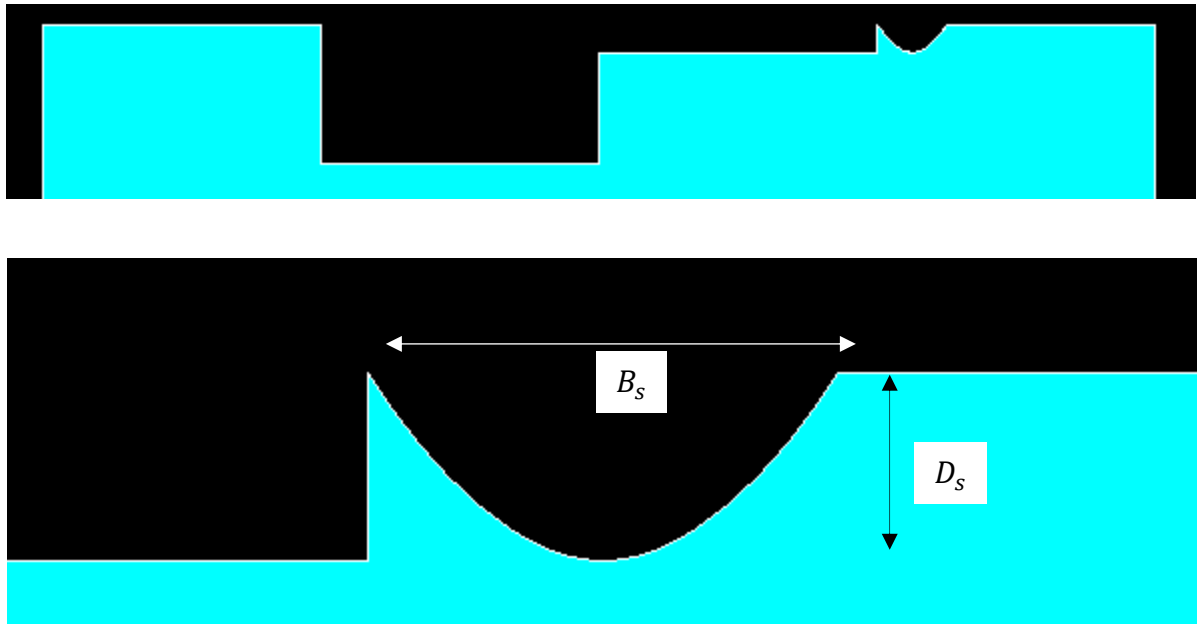


Fig. 5. Dimensions of the scour at the toe of the stilling basin

Table 9. Results of convergence study using 4-noded elements

Uniform Mesh					Adaptive Mesh
Mesh	Element Size, h (m)	Maximum Exit Gradient	Computing Time	Relative Error	Maximum Exit Gradient
1	2	0.4167	t		0.5462 (508t)
2	1	0.4993	3t	19.81 %	
3	0.5	0.4950	10t	0.86 %	
4	0.25	0.5218	42t	5.41 %	
5	0.125	0.5366	225t	2.85 %	

Table 10. Results of convergence study using 6-noded elements

Uniform Mesh					Adaptive Mesh
Mesh	Element Size, h (m)	Maximum Exit Gradient	Computing Time	Relative Error	Maximum Exit Gradient
1	2	0.4764	t		0.5545 (8t)
2	1	0.5529	2t	16.06 %	
3	0.5	0.5541	7t	0.22 %	
4	0.25	0.5532	28t	0.16 %	
5	0.125	0.5542	138t	0.18 %	

Table 11. Results of convergence study using 8-noded elements

Uniform Mesh					Adaptive Mesh
Mesh	Element Size, h (m)	Maximum Exit Gradient	Computing Time	Relative Error	Maximum Exit Gradient
1	2	0.5415	2t		0.5538 (12t)
2	1	0.5632	3t	3.99 %	
3	0.5	0.5488	17t	2.54 %	
4	0.25	0.5517	47.2t	0.53 %	
5	0.125	0.5538	253t	0.38 %	

For weir with a scour, based on optimal combination of efficiency and accuracy, 6-noded triangular element with adaptive meshing yield better results than 4-noded and 8-noded elements as the 6-noded triangular element is able to accurately represents the curved boundary profile of the scour.

The effect of downstream water depth on the maximum exit gradient in the scour profile is given in Table 12. As the downstream water level increases, the exit gradient decreases due to decrease in differential head in water levels between the upstream and the downstream sides of the weir structure.

The seepage analysis is also carried out for different scour profiles by varying the depth and the width of the scour. Table 13 shows the maximum exit gradient for different scour

profiles. It is observed that the maximum exit gradient increases with increase in the scour depth and decrease in the scour width, which can lead to rupture failure much faster.

Table 12. Effect of Downstream water level on Maximum Exit Gradient

Downstream water level <i>H_{d/s} (m)</i>	Maximum Exit Gradient
0	0.5545
0.5	0.5293
1	0.5041
1.5	0.4789
2	0.4537

Table 13. Maximum Exit Gradient for different scour profiles

Scour width, <i>B_s</i> (m)	Scour depth, <i>D_s</i> (m)	Maximum Exit Gradient
2	0.5	0.5854
	1	0.8045
	1.5	1.0513
3	0.5	0.4836
	1	0.6228
	1.5	0.7508
	2	0.8513

Table 13 Continued

4	1	0.5183
	1.5	0.5989
	2	0.6668
	2.5	0.7120
5	1	0.4596
	1.5	0.5116
	2	0.5545
	2.5	0.5868

6. Flooding Fragility Analysis

Flooding fragility curves are essential tools for assessing the vulnerability of a particular flood defense structure, and offer a means of communicating the probability of damage over a range of potential flooding levels. Fragility of a component or structure is defined as the conditional probability of failure, $P_{f|\lambda}$, to exceed a defined performance function, Z , at a given measure of intensity parameter λ e.g. flooding height. The performance function for this analysis is defined in section 2.3.

Fragilities are evaluated by considering uncertainties in variables that are used to characterize the local soil characteristics such as the anisotropic ratio, porosity, and specific gravity. The statistical distributions for the variables (Sandhu, 2015) incorporated in this study are shown in Fig. 6. A set of 250 random samples are generated from each of these normally distributed parameters. The analysis is carried out for such 250 random simulations with

different heights of upstream water level ranging from 0 to 11 meters to calculate the probability of rupture failure. The fragility data is fitted to a cumulative lognormal distribution using maximum likelihood estimation.

Variation in fragility curves for different scour profiles by varying the scour width ($B_s = 2, 3, 4 \text{ m}$) with a fixed scour depth ($D_s = 1.5 \text{ m}$) and varying the scour depth ($D_s = 1, 1.5, 2 \text{ m}$) with a fixed scour width ($B_s = 3 \text{ m}$) are shown in Figs. 7 and 8 respectively.

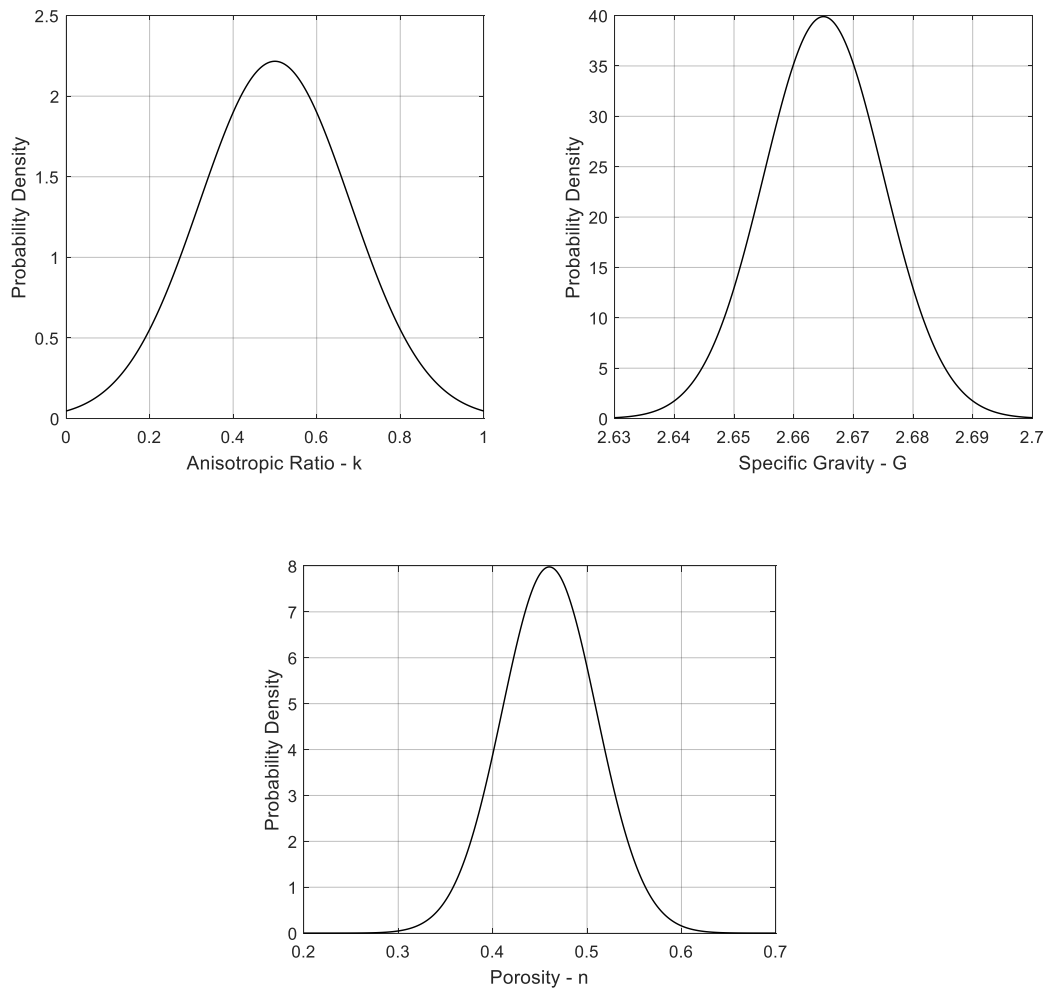


Fig. 6. Distributions of the random variables used to evaluate fragility curves

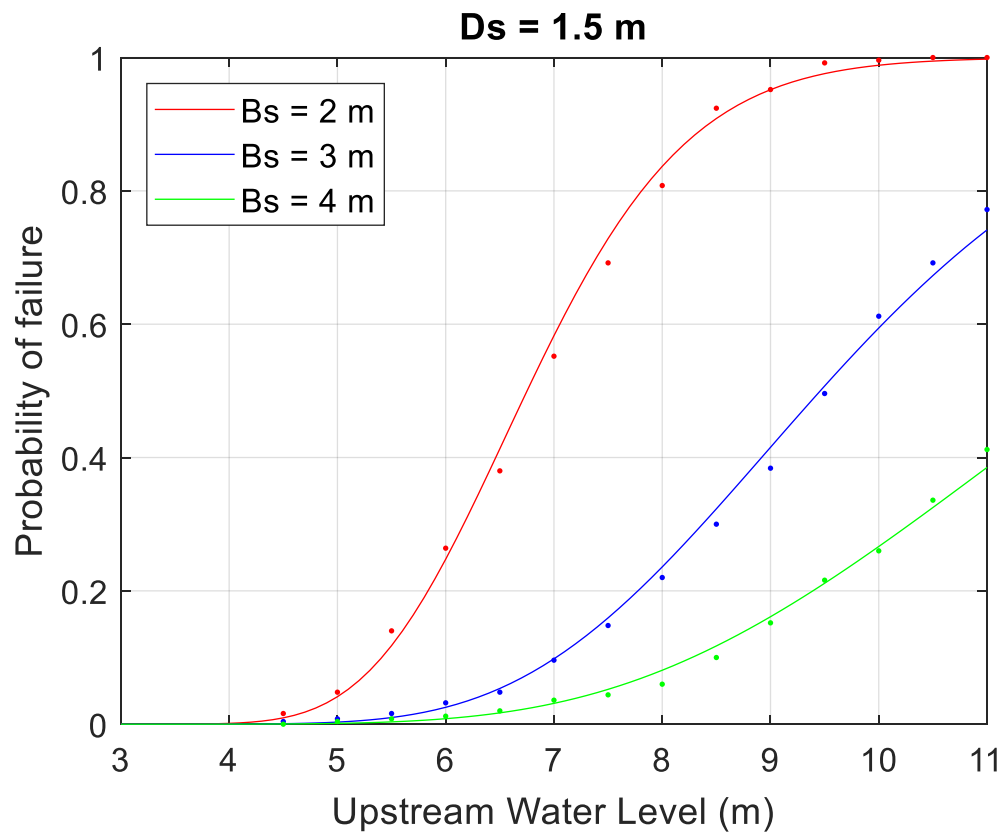


Fig. 7. Fragility curves for rupture failure for fixed $D_s = 1.5 \text{ m}$ and varying $B_s = 2, 3, 4 \text{ m}$

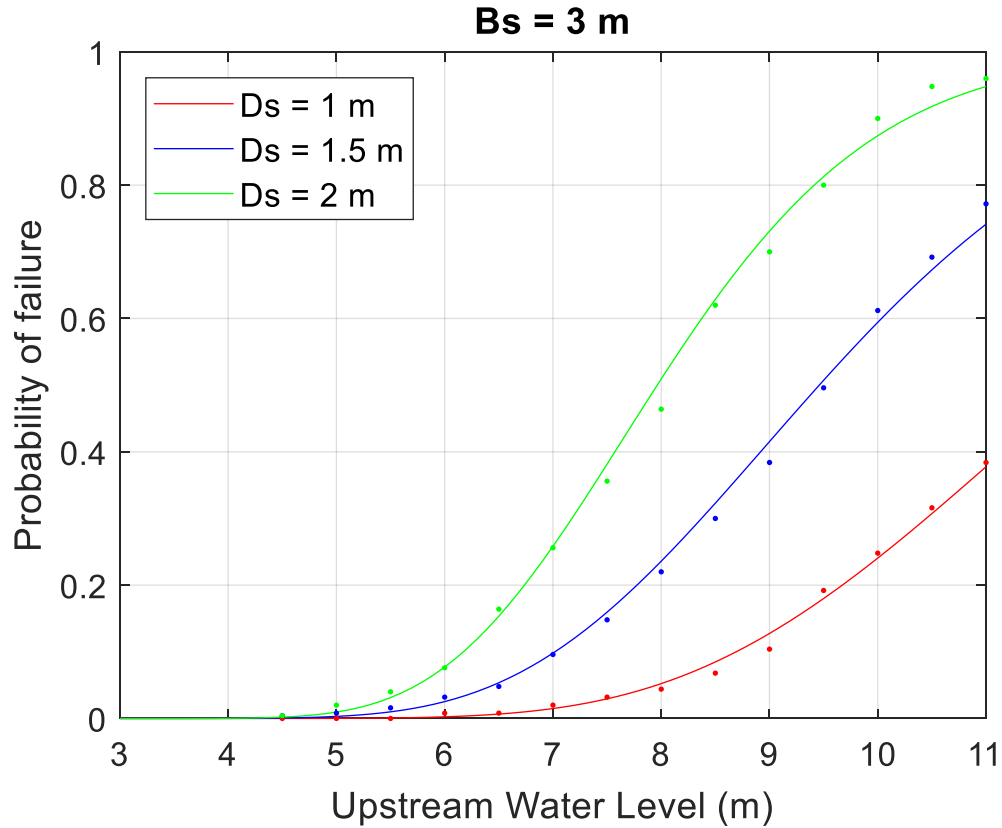


Fig. 8. Fragility curves for rupture failure for fixed $B_s = 3 \text{ m}$ and varying $D_s = 1, 1.5, 2 \text{ m}$

The probability of rupture failure decreases with the increase in scour width for the same scour depth due to increase in distance between the toe of the stilling basin and the location of maximum scour depth. For scour profiles with fixed scour width, the rupture probability increases with increase in the scour depth.

7. Conclusions

Uncontrolled seepage can lead to piping or undermining subsequently resulting in a rupture failure of the foundation. Local scour downstream of stilling basins can initiate the rupture failure much faster. The uncertainties in random variables influencing the rupture failure are incorporated and the rupture fragility curves for various scour profiles are obtained.

The key conclusions are:

- 6-noded triangular and 8-noded quadrilateral elements are better choice compared to conventional 4-noded quadrilateral elements for a seepage analysis.
- Advanced mesh techniques such as adaptive mesh refinement are reduce the computational cost significantly.
- The anisotropic ratio (k_y/k_x) has a significant effect on the calculation of exit gradient. As the anisotropic ratio decreases, the exit gradient increases, thereby, the chances of rupture failure are increased.
- The proper location for the truncation boundary condition to represent the elastic half-space is investigated. According to the convergence analyses, the upstream width (B_1), the downstream width (B_2), and the depth (D) of the elastic half space should be at least 2.5 times more than the combined width of the weir structure and the stilling basin.
- For a constant upstream flood level, the probability of rupture failure decreases with the increase in scour width for the same scour depth. As the scour depth increases with time, the exit gradient increases with a consequent risk to failure of the structure.

REFERENCES

- Bardet, J. P., and Tobita, T. (2002). "A practical method for solving free-surface seepage problems," *Computers and Geotechnics*, 29(6), 451-475.
- Billstein, M., Svensson, U., and Johansson, N. (1999). "Development and Validation of a Numerical Model of Flow Through Embankment Dams – Comparisons with Experimental Data and Analytical Solutions," *Transport in Porous Media*, 35(3), 395–406.
- Broaddus, M. R. (2015). "Performing a steady-state seepage analysis using SEEP/W : a primer for engineering students," Electronic Theses and Dissertations. Paper 2219.
- CNBC, 2017. "<https://www.cnbc.com/2017/08/30/arkema-ceo-no-way-to-potentially-stop-an-explosion.html>"
- Dehghani, A. A., Bashiri, H., and Meshkati, S. M. E. (2010). "Local scouring due to flow jet at downstream of rectangular sharp-crested weirs," *Water and Geoscience*, 5th IASME WSEAS, Cambridge, UK, 127–131 (ISSN: 1790-5095).
- Elnikhely, E. A. (2017). "Investigation and analysis of scour downstream of a spillway," *Ain Shams Engineering Journal*.
- Farhoudi, J. and Shayan, H. K. (2014). "Investigation on Local Scour Downstream of Adverse Stilling Basins," *Ain Shams Engineering Journal*, 5, 361-375.
- FEMA P-1090 / DR-4285-NC. (2017). "Hurricane Matthew in North Carolina Dam Risk Management Assessment Report."

- Hasani, H., Mamizadeh, J., and Karimi, H. (2013). "Stability of Slope and Seepage Analysis in Earth Fills Dams Using Numerical Models (Case Study : Ilam Dam- Iran)," *World Applied Sciences Journal*, 21(9).
- International Atomic Energy Agency (IAEA). (2015). "The Fukushima Daiichi Accident."
- Ju, B. S., and Jung, W. (2015). "Evaluation of Seismic Fragility of Weir Structures in South Korea," *Mathematical Problems in Engineering*, 10 pages.
- Kirra, M. S., Zeidan, B. A., Shahien, M. M., and El-Shemy, M. (2015). "Seepage Analysis of Walter F. George Dam, USA: A case Study," *International Conference on Advances in Structural and Geotechnical Engineering*, 6-9 April 2015, Hurghada, Egypt.
- Kolawole, A. O. and Oluwole A. A. (2013). "A Study of Seepage through Oba Dam Using Finite Element Method," *Civil and Environmental Research*, 3, 3 (ISSN 2222-1719).
- Kratochvil, J. and Bachorec, T. (2004). "Numerical modeling of Non stationary Free Surface Flow in Embankment Dams," Brno University of Technology, CZ.
- Naouss, W. A. and Najjar, Y. M. (1995). "Seepage design charts for flat bottom dams resting on heterogeneous media," *International Journal for Numerical and Analytical Methods in Geomechanics*, 19, 637–651.
- Noori, B. A. and Ismaeel, K. S. (2011). "EVALUATION OF SEEPAGE AND STABILITY OF DUHOK DAM," *Al-Rafadain Engineering Journal*, 19(1), 42-58.
- Oliveto, G., and Comuniello, V. (2010). "Local scour progress downstream of low-head stilling basins," University of Basilicata, Italy.

- Robert, K., Brian C., and Helen, G. (2006). "USGS Scientists Investigate New Orleans Levees Broken by Hurricane Katrina," *USGS Sound Waves Monthly Newsletter*.
- Saleh, I. K., Aqeel, S. A., and Rafid, and S. R. (2009). "Seepage Analysis underneath Diyala Weir Foundation," *Thirteenth International Water Technology Conference, IWTC 13 2009, Hurghada, Egypt*.
- Sandhu, H. K. (2015). "Flooding Fragility of Concrete Gravity Dam-Foundation System," Master of Science Thesis, Department of Civil Engineering, North Carolina State University, Raleigh, NC.
- Soleymani, S. and Akhtarapur, A. (2011). "Seepage Analysis for Shurijeh Reservoir Dam Using Finite Element Method," *Geo-Frontiers Congress, American society of civil engineering*.
- U.S. Army Corps of Engineers. (1993). "Seepage Analysis and Control for Dams," EM 1110-2-1901.

PART III: MULTI-HAZARD FRAGILITY ASSESSMENT OF A CONCRETE

FLOODWALL

1. Introduction

The March 2011 Fukushima Daiichi nuclear power plant disaster has highlighted the significance of maintaining the integrity of flood protection systems in the vicinity of a nuclear power plant. In the US, Fort Calhoun nuclear plant was shut down when the floodwall protecting vital areas at the plant against the historic flood on Missouri river collapsed. Nuclear plants are typically located near a body of water such as a river, lake, an estuary or sea because they require abundant and dependable source of water for cooling. These nuclear facilities can be protected from floods through the use of flood protection systems such as floodwalls, dams, and weirs. In rare cases, seismically induced failure of flood defense structures would result in flooding at the nuclear plant. For developing the flooding probabilistic risk assessment (PRA) for nuclear power plants, it is essential to evaluate the risk of flood protection systems under multi-hazard scenario. The two key components for calculating the risk of a flood defense structure are the fragility (probability of failure) and the hazard. In order to obtain the fragility of a flood defense structure, all critical failure modes must be accounted for and adequately expressed to represent the failure through the use of performance functions.

Various studies have been performed in the past to evaluate the fragilities for failure of flood defense structures under flooding and seismic events. Tekie and Ellingwood (2003) presents a methodology for developing seismic fragility and flooding fragility of concrete gravity dams. Lupoi (2012) uses a similar approach to conduct the seismic fragility analysis of the Kasho dam. Ju and Jung (2015) conduct seismic probabilistic risk assessment and its application to the case of the Gangjeong-Goryeong weir in Korea. Kaida and Miyagawa (2016) describes a methodology for evaluating fragility of a seawall against tsunami. Rajabalinejad et

al. (2008) uses a probabilistic method integrated with finite element analysis to estimate the probability of failure of 17th street floodwall of New Orleans.

However, there are no existing studies on probabilistic safety assessment (PSA) of a concrete floodwall considering a comprehensive set of failure modes particularly under a multi-hazard scenario. Furthermore, the effects of hydrodynamic pressure and seepage under the foundation have not been considered in the existing studies.

In this paper, we present the results from a study on evaluating the fragilities for failure of a concrete flood wall due to various failure modes under a multi-hazard scenario. The failure modes considered for flooding loads are rigid body failure and foundation failure. Rigid body failure is characterized by sliding and overturning of the floodwall. Failure of floodwall foundation is characterized by rupture and compression failure at the toe. For seismic loads, the structural failure of floodwall is characterized by excessive deformation. Finite element analysis is used for modeling the seismic behavior as well as the seepage through the foundation. Fragilities are evaluated by considering uncertainties in several variables that are used to characterize the earthquake input, reservoir levels, flood wall geometry, material properties, and local soil characteristics. A multi-hazard assessment of flooding and earthquake results in the evaluation of a fragility surface because both the flood hazard and seismic performance are correlated through the height of water in the reservoir. Such a fragility surface due to combined seismic and flooding events is evaluated in this paper.

2. Problem Description

The failure of a floodwall during extreme flooding is typically a function of the height of reservoir pool. Higher water levels in the pool result in higher gradient for seepage through the foundation and the consequent chances of a foundation failure are thereby increased. At the same time, the earthquake behavior of a floodwall is highly dependent upon the fluid-structure interaction between the water pool and the concrete structure. A higher level of reservoir results in greater hydrodynamic pressure leading to greater chances of failure. The study presented in this research is carried out for a simple model of a floodwall.

3. Flooding Fragility Analysis

3.1 Failure in Stability

A floodwall can fail by rigid body failure mechanism (either due to overturning or sliding), or crushing failure of the foundation or concrete. Fig. 1 shows the loads that are normally considered for the stability analysis of a floodwall and are described below.

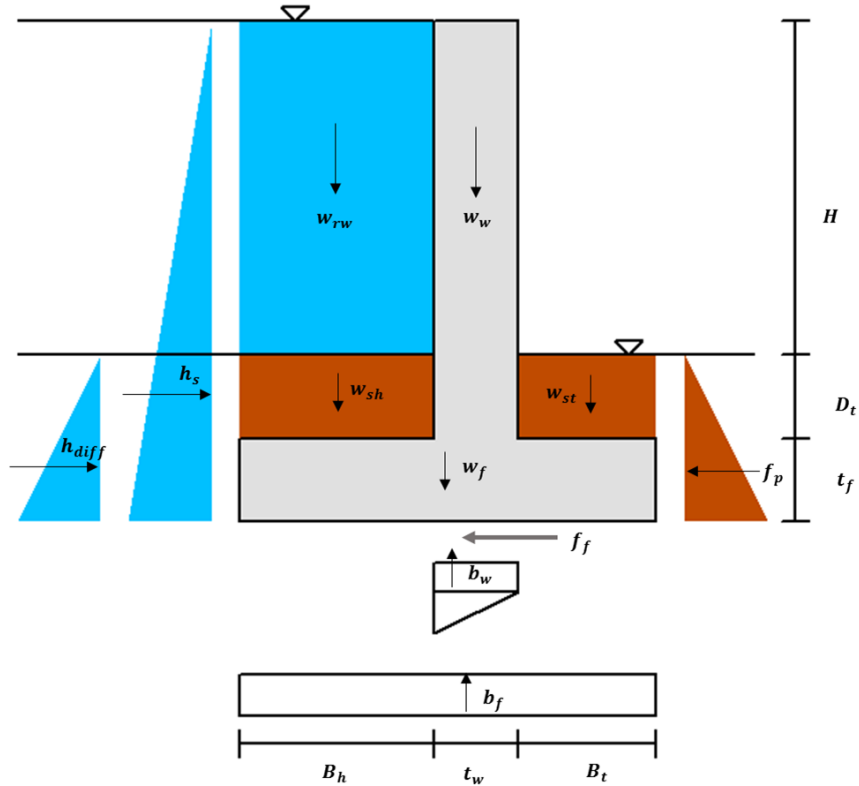


Fig. 9. Loads acting on the floodwall

- | | | | |
|-------|------------------------------------|------------|---|
| B | = footing width | γ_c | = specific weight of concrete |
| H_w | = wall height | γ_w | = specific weight of water |
| H | = upstream water level | γ_s | = specific weight of soil |
| t_w | = wall thickness | k_p | = passive soil pressure coefficient |
| t_f | = footing thickness | G_s | = specific gravity of soil |
| D_t | = depth of the soil above the toe | H_{ds} | = downstream water level |
| D_h | = depth of the soil above the heel | S | = equivalent fluid weight of submerged soil and water |
| B_t | = toe width | | |
| B_h | = heel width | | |

3.1.1 Loads acting on the Floodwall

a. Gravity Load: The gravity load acting downward is taken to be the total weight of the flood wall, retaining water above the heel, and weight of the soil over the heel and the toe. The weight of the section per unit length is equal to the area of the cross section times the specific weight of the material. The load acts vertically downwards through the center of gravity of the sections as shown in Fig. 1.

$$\text{weight of the wall (N/m)} \quad : \quad w_w = H_w t_w \gamma_c \quad (1)$$

$$\text{weight of the footing (N/m)} \quad : \quad w_f = B t_f \gamma_c \quad (2)$$

$$\begin{array}{l} \text{weight of the retaining water above the heel} \\ \text{(N/m)} \end{array} \quad : \quad w_{rw} = (H + D_h) B_h \gamma_w \quad (3)$$

$$\text{weight of the soil over the heel (N/m)} \quad : \quad w_{sh} = D_h B_h (\gamma_s - \gamma_w) \quad (4)$$

$$\text{weight of the soil over the toe (N/m)} \quad : \quad w_{st} = D_t B_t \gamma_s \quad (5)$$

b. Hydrostatic Forces: Water that lies below or above the ground surface causes hydrostatic loads. Various types of loads that contributes to the hydrostatic loads are lateral hydrostatic loads, uplift loads at the bottom of foundation, and differential saturated soil force acting in the horizontal direction beneath the ground surface. Hydrostatic pressures increase linearly with the depth of water above or below the point under consideration and are equal in all directions.

$$\text{lateral hydrostatic force (N/m)} \quad : \quad h_s = 0.5 \gamma_w (H + D_h + t_f)^2 \quad (6)$$

$$\begin{array}{l} \text{differential saturated soil/water force} \\ \text{(N/m)} \end{array} : \quad h_{diff} = 0.5(S - \gamma_w)(D_h + t_f)^2 \quad (7)$$

$$\text{buoyancy force on the footing (N/m)} : \quad b_f = \gamma_w B t_f \quad (8)$$

$$\text{buoyancy force on the wall (N/m)} : \quad b_w = 0.5\gamma_w t_w (H + D_t + D_h) \quad (9)$$

c. Frictional Force: The sliding frictional force, f_f acting along the base of the foundation is proportional to the net vertical force f_v and the coefficient of friction is represented as μ_f .

$$\begin{array}{l} \text{frictional force} \\ \text{(N/m)} \end{array} : \quad \begin{array}{l} f_f = f_v \mu_f \\ f_v = (w_w + w_f + w_{rw} + w_{sh} + w_{st}) - (b_w + b_f) \end{array} \quad (10)$$

d. Lateral Passive Earth Force: The passive earth pressure is generated when the soil mass is compressed outward due to the pushing of floodwall on it.

$$\begin{array}{l} \text{passive saturated soil force} \\ \text{(N/m)} \end{array} : \quad f_p = 0.5[k_p(\gamma_s - \gamma_w) + \gamma_w](D_t + t_f)^2 \quad (11)$$

3.1.2 Performance Functions

In this study, three performance functions are used to characterize the stability failure and evaluate the corresponding fragilities. These three performance functions are described below.

a. Sliding Failure: Sliding failure occurs if the horizontal forces due to lateral hydrostatic loads exceeds floodwall resistance due to frictional and passive soil loads, thereby causing the floodwall to slide horizontally as an entire unit as shown in Fig. 2. The performance function for sliding failure is characterized by following limit state:

$$Z_s = \sum R_H - \sum F_H \quad (12)$$

$$\sum R_H = f_p + f_f \quad \sum F_H = h_s + h_{diff} \quad (13)$$

where: $\sum R_H$ is the total resistive force, $\sum F_H$ is the total horizontal force

The probability of failure due to sliding of the flood wall is given by:

$$P_f(\text{sliding}) = P(Z_s < 0) \quad (14)$$

b. Overturning of the flood wall: Wall overturning occurs if the overturning moments due to the hydrostatic forces exceeds the floodwall resistive moments due to all vertical downward forces and passive soil load about the toe, thereby causing the floodwall to topple or rotate as shown in Fig. 2. The performance function for overturning failure is characterized by following limit state:

$$Z_o = \sum M_R - \sum M_O \quad (15)$$

where: $\sum M_R$ is the total resisting moments about the toe, and $\sum M_O$ is the overturning moments

$$\begin{aligned} \sum M_R = & w_w(A_t + 0.5t_w) + w_f(0.5B) + w_{sh}(B - 0.5A_h) + w_{st}(0.5A_t) \\ & + w_{rw}(B - 0.5A_h) + f_p \left(\frac{D_t + t_f}{3} \right) \end{aligned} \quad (16)$$

$$\sum M_o = h_s \left(\frac{H + D_h + t_f}{3} \right) + h_{diff} \left(\frac{D_h + t_f}{3} \right) + b_f(0.5B) + b_{w1}(A_t + 0.5t_w) + b_{w2} \left(\frac{2}{3}t_w + A_t \right) \quad (17)$$

The probability of failure due to overturning of the floodwall is given by:

$$P_f(\text{overturning}) = P(Z_o < 0) \quad (18)$$

c. Compression failure of foundation at the toe of the floodwall: Compression failure of the foundation at the toe occurs if the pressure on the foundation, p_n exceeds the allowable soil bearing capacity, σ_b^f . The performance function for compression failure of foundation at toe is characterized by following limit state:

$$Z_{cf} = \sigma_b^f - p_n \quad (19)$$

$$p_n = \frac{f_v}{B} \left(1 + \frac{6e}{B} \right) \quad (20)$$

where, distance e is the eccentricity from the centerline of the footing and represents the location of resultant force.

$$e = \frac{B}{2} - \frac{M_R - M_O}{f_v} \quad (21)$$

The probability of failure of foundation due to compression at toe is given by:

$$P_f(\text{compression_toe}) = P(Z_{cf} < 0) \quad (22)$$

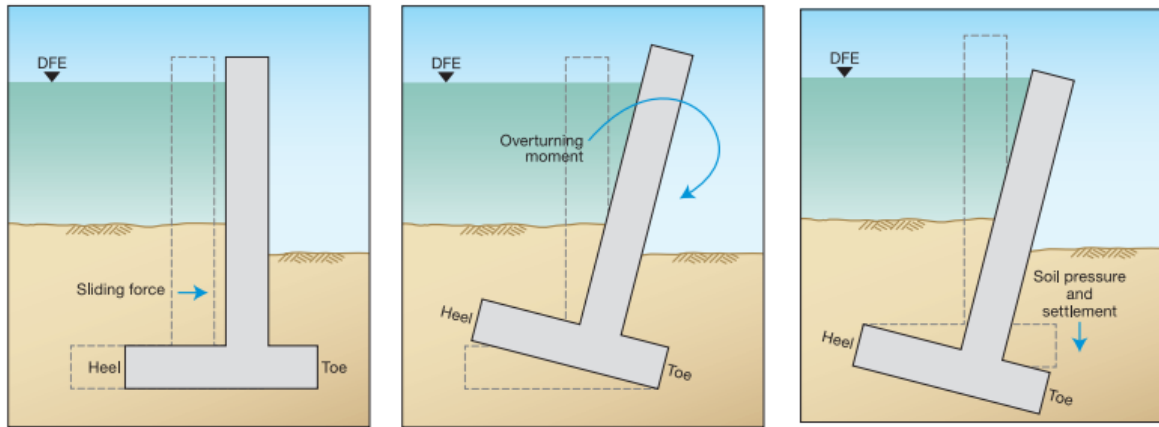


Fig. 10. Failure by sliding, overturning, and compression failure of foundation (FEMA259, 2012)

3.1.3 Fragility Curves for Stability failure

Fragility curves are one of the key components of probabilistic risk assessment. Fragility curve gives the conditional probability of failure over the complete range of loads to which that system might be exposed in its lifetime. The uncertainties in the random variables that characterizes the performance function are incorporated using Monte Carlo simulations. The parameters to be taken as random variables are chosen in accordance with the existing studies (Sandhu, 2015; FEMA-259, 2012) and are shown in Table 1. The analysis is carried out for 100,000 random samples with different heights of upstream water level ranging from 0 to 5 meters to calculate the probability of failure. Fragility curves due to sliding failure are shown in Fig. 3 and fragility curves due to compression failure of foundation at toe are shown in Fig. 4. The fragility curves are generated for two classes of soils, Class-2 and Class-3 according to the Table 3285.202 of ASTM D 2487-00. The soil foundation at the site consists of silty sand which belongs to Class-3.

The fragility curve due to sliding failure for class-3 soil shows greater uncertainty than the class-2 soil due to larger uncertainty in coefficient of friction for class-3 soil. The fragility curves are not plotted for overturning failure mode as the total resistive moments are greater than the overturning moments. The fragility curves for compression failure of foundation at the toe are governed by the allowable soil bearing capacity.

Table 14. Random variables and deterministic values used to evaluate fragility curves

Variable	Distribution	Parameters/moments
H_{ds} (m)	Deterministic	0
g (m/s ²)	Deterministic	9.81
S (kN/m ³)	Normal	<i>Soil Class – 2</i> : $\mu_S = 12, \sigma_{C_f} = 0.12$ <i>Soil Class – 3</i> : $\mu_{C_f} = 13, \sigma_{C_f} = 0.195$
γ_w (kN/m ³)	Deterministic	9.804
γ_c (kN/m ³)	Normal	$\mu_{\gamma_c} = 25,$ $\sigma_{\gamma_c} = 1$
G_s (-)	Normal	$\mu_{G_s} = 2.66,$ $\sigma_{G_s} = 0.01$
μ_f (-)	Normal	<i>Soil Class – 2</i> : <i>Uniform</i> [0.55 0.60] <i>Soil Class – 3</i> : <i>Uniform</i> [0.35 0.55] <i>Silty Sand</i> : <i>Uniform</i> [0.45 0.55]
k_p (-)	Normal	$\mu_{k_p} = 3.5,$ $\sigma_{k_p} = 0.3$
σ_b^f (kN/m ²)	Normal	<i>Soil Class – 2</i> : $\mu_{k_p} = 95, \sigma_{k_p} = 2$ <i>Soil Class – 3</i> : $\mu_{k_p} = 70, \sigma_{k_p} = 2$
$D_t = D_h$ (m)	Deterministic	0

where: μ is the mean, σ is the standard deviation

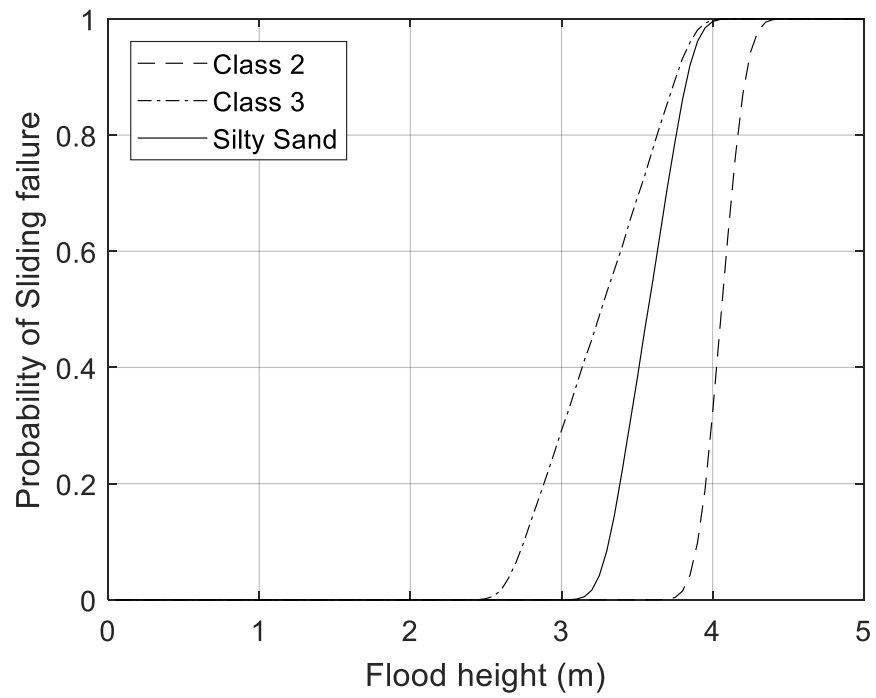


Fig. 11. Fragility curve due to sliding failure

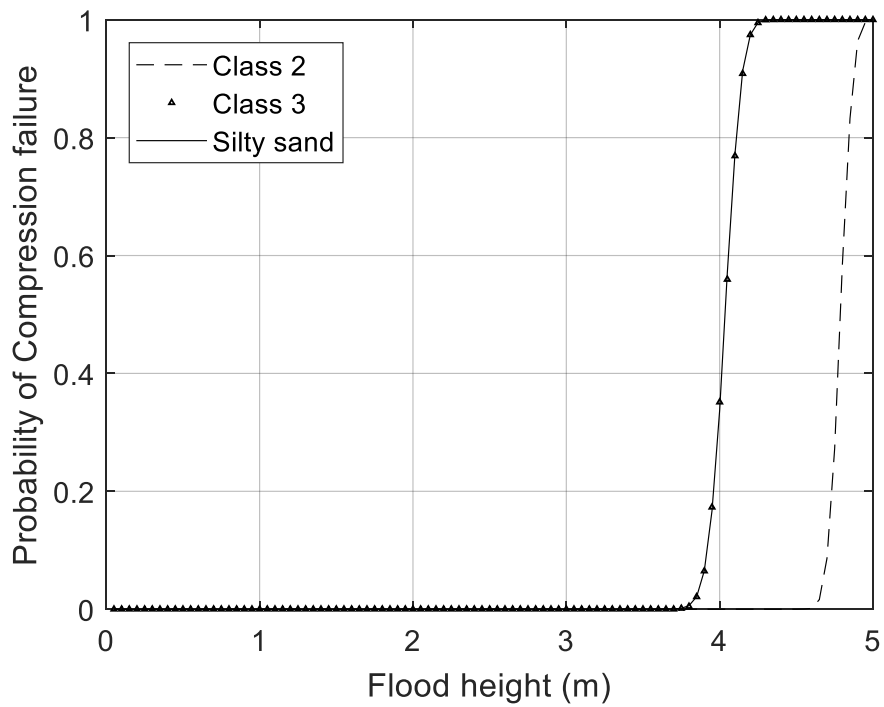


Fig. 12. Fragility curve due to compression failure of foundation at toe

3.2 Failure in Instability

Seepage analysis plays an important role in the design of flood defense structures. Uncontrolled seepage can cause excessive uplift pressures, and internal erosion of the material at the downstream leading to the piping through the embankment and the foundation. Piping phenomenon is initiated when the rupture of the foundation occurs and the rupture takes place if the critical hydraulic gradient (i_{cr}) is lesser in magnitude than the maximum exit gradient (i_{ex}). For the accurate calculation of seepage gradients under the flood defense structures, numerical methods are usually adopted. In this study, finite element method is used for solving the seepage problem as it can capture the effects of complex boundaries and soil anisotropy accurately.

Based on Darcy's law, the discharge velocity for a homogeneous, anisotropic soil is given by:

$$v_n = -k_n \frac{\partial h}{\partial n} \quad (23)$$

where: v is the discharge velocity or seepage flow, h is the total hydraulic head, and k is the hydraulic conductivity.

The differential equation governing the steady-state flow is expressed as:

$$k_x \frac{\partial^2 h}{\partial x^2} + k_y \frac{\partial^2 h}{\partial y^2} = 0 \quad (24)$$

For the critical hydraulic gradient, the following expression by Terzaghi (1943) is used:

$$i_{cr} = \frac{G - 1}{1 + e} = (G - 1)(1 - n) \quad (25)$$

where: G is the specific gravity of the soil, n and e are the porosity and void ratio of the soil.

The governing equations and boundary conditions to be applied in order to solve the two-dimensional partial differential equation of the seepage problem are shown in Fig. 5 and discussed below:

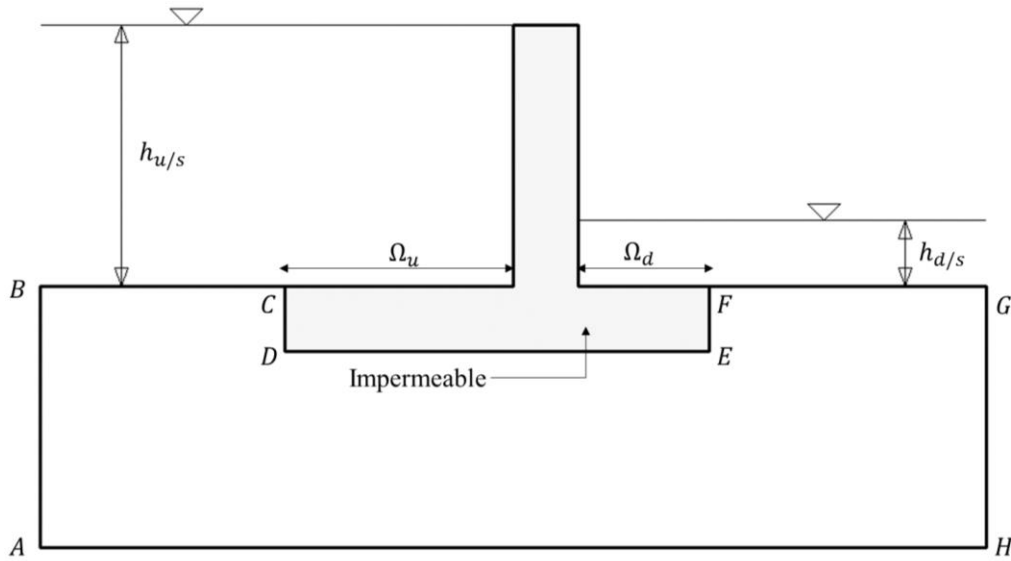


Fig. 13. Boundary conditions for the seepage analysis

Hydraulic head boundary conditions: Hydraulic head on the upstream side (BC and Ω_u) of the floodwall is equal to the upstream water level, $h_{u/s}$. Hydraulic head on the downstream side (FG and Ω_d) of the floodwall is equal to the downstream water level, $h_{d/s}$.

$$h = h_{u/s} \text{ on } BC \text{ and } \Omega_u, \quad h = h_{d/s} \text{ on } FG \text{ and } \Omega_d$$

Seepage flow boundary conditions: No flow boundary conditions are imposed on the impermeable concrete floodwall (CD, DE, EF) and the elastic half space (AB, GH, AH).

$$k_n \frac{\partial h}{\partial n} = 0 \text{ on } AB, CD, DE, EF, GH, AH.$$

Fragility Curve for Rupture failure

The finite element model for the seepage analysis is developed by following the concepts described in part II of this thesis. Based on the convergence study, the dimensions of the elastic half space are found out to be: upstream width, $B_1 = 15 \text{ m}$; downstream width, $B_2 = 15 \text{ m}$; depth, $D = 20 \text{ m}$.

In this study for calculating the probability of rupture failure, uncertainties in both the capacity and the demand are considered. The capacity, critical gradient is a function of specific gravity and porosity of the soil. The demand, maximum exit gradient is a function of anisotropic ratio (k_y/k_x) and upstream flood water level.

The limit state equation or performance function is expressed as the difference between capacity, i_{cr} , and demand, i_{ex} :

$$Z_R = i_{cr} - i_{ex} \quad (26)$$

The conditional probability of rupture failure given upstream flood water level (H) is expressed as:

$$P_f(\text{rupture}|H) = P(Z_R < 0) \quad (27)$$

The fragility curve is generated using Monte Carlo simulation by considering all the uncertainties in both the capacity and the demand (Table. 2). A set of 200 random samples are generated from each of the random variables. The fragility analysis is carried out for such 200 samples per each upstream water level ranging from 0 to 5 m. The fragility curve due to rupture failure is shown in Fig. 6.

Table 15. Random variables and deterministic values used to evaluate fragility curves

Variable	Distribution	Parameters/moments
k_y/k_x (-)	Normal	$\mu_K = 0.5$ $\sigma_K = 0.18$
n (-)	Normal	$\mu_n = 0.46$ $\sigma_n = 0.05$
G_s (-)	Normal	$\mu_G = 2.66$ $\sigma_G = 0.01$

where: μ is the mean, σ is the standard deviation, H_{ds} – Height of downstream water level

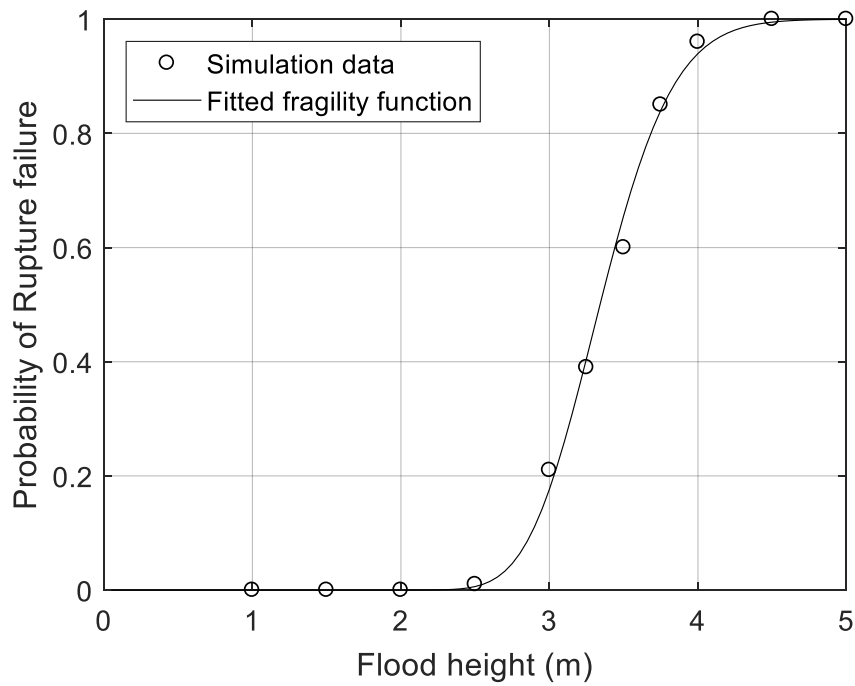


Fig. 14. Fragility curve due to rupture failure

3.3 System Level Flooding Fragility

The system level flooding fragility is evaluated by considering the effect of all the failure modes of a floodwall. Considering all these modes as independent, the combined fragility of failure due to flooding hazard is calculated using the following expression:

$$P(\text{system}|\text{flood height}) = \bigcup_i P(LS_i|\text{flood height}) \quad (28)$$

where, $P(LS_i|\text{flood height})$ is the fragility of i^{th} failure mode.

The system level flooding fragility curve is shown in Fig. 7. The failure probability for system level at different flood heights is governed by different failure modes. Rupture failure mode governs until a flood height of 3.3 m and sliding failure mode governs after a flood height of 4 m. In this analysis, the effect of compression failure mode is negligible as compared with other failure modes.

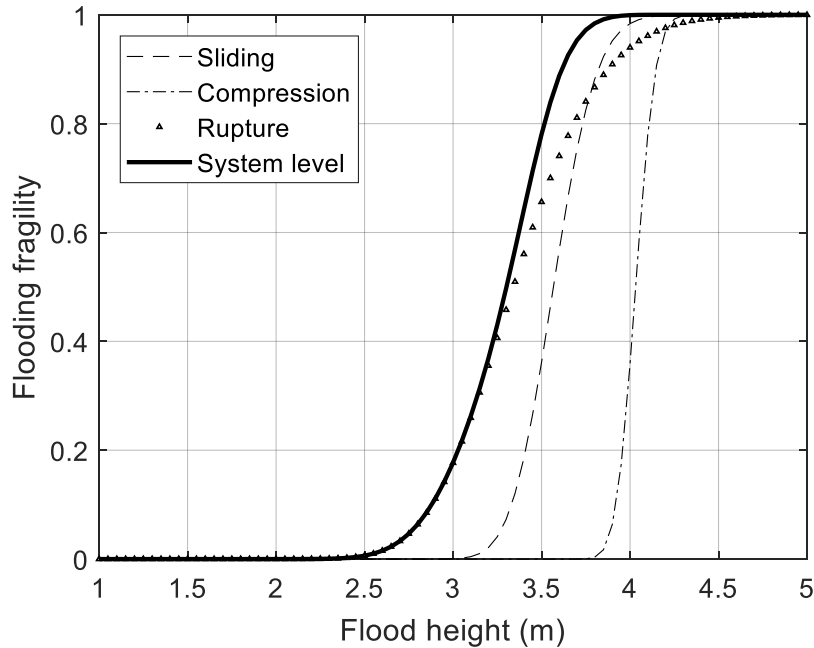


Fig. 15. System level flooding fragility curve

4. Seismic Fragility Analysis

In this section, the effect of various ground motions on the seismic response of floodwalls is investigated. Finite element analysis is used for modeling the seismic behavior of the floodwall. The modeling concepts described in detail in Bodda et al. (2016) for the analysis of a concrete gravity dam are used for modeling the floodwall. The formulations and associated concepts are discussed below.

4.1 Fluid Structure Interaction (FSI) Formulation

A large number of existing studies assume that the fluid is incompressible in a fluid-structure interaction analysis. However, Akhaveiss and Malekshahi (2012) illustrate that consideration of fluid compressibility in such analyses results in higher hydrodynamic pressures on the upstream face of the structure. Therefore, fluid is modeled as compressible in the study described below.

The two dimensional wave equation for a fluid is obtained from the combined Navier-Stokes equations of fluid momentum and the flow continuity equation by assuming that fluid is compressible. Compressibility is defined as changes in fluid density due to pressure variations. The viscosity is neglected and the mean density and pressure are considered to be uniform throughout the fluid:

$$\frac{1}{c^2} \frac{\partial^2 P}{\partial t^2} - \nabla^2 P = 0 \quad (29)$$

where, $P = P(x, y, t)$ is the acoustic pressure, c is the acoustic wave speed, and t is the time. If the fluid is incompressible then Eq. (29) simplifies to:

$$\nabla^2 P = 0 \quad (30)$$

Eq. (23) is used to solve the fluid-structure interaction problem by imposing the following boundary conditions (Khosravi and Heydari, 2013) on the fluid domain as shown in Fig. 8.

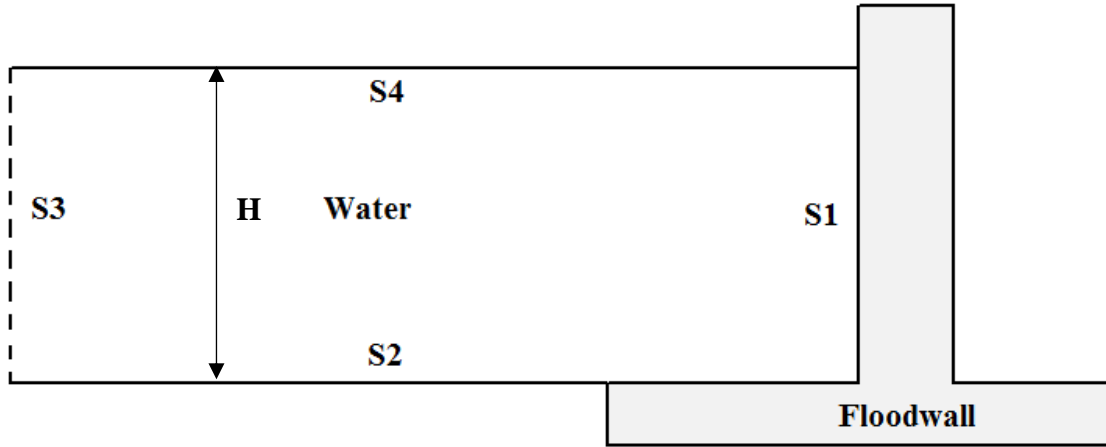


Fig. 16. Boundary conditions of the fluid domain

Fluid Boundary Conditions

Fluid-Structure Interface (S1) – At this boundary, the pressure gradient is equal to the inertial force caused by the movement of reservoir wall. Therefore,

$$\frac{\partial P}{\partial n} = -\rho \ddot{U}_n \quad (31)$$

where n is the unit vector normal to the interface, \ddot{U}_n is the normal acceleration of structure at the interface.

Reservoir bottom (S2) – It is assumed that the incident hydrodynamic pressure waves gets absorbed by the material at the bottom of reservoir bottom. To account for this assumption at boundary S2, a damping coefficient \bar{q} is incorporated.

$$\frac{\partial P}{\partial n} = -\rho \ddot{U}_n - \bar{q} \frac{\partial P}{\partial t}, \quad \alpha = \frac{1 - \bar{q}c}{1 + \bar{q}c} \quad (32)$$

where α is the wave reflection coefficient, defined as the ratio of the amplitude of the reflected pressure wave to that of the normally incident wave. The value of α is typically selected based on the properties of material that forms the reservoir bed. A value of α equal to zero represents a soft reservoir bed such that all the waves are absorbed and a value of 1 represents a rigid foundation such that all the waves are reflected back (Fenves and Chopra, 1983).

Reservoir upstream boundary (S3) – At this boundary, the outgoing hydrodynamics waves generated due to the vibration of wall should continue to propagate outward but not inward. This condition is termed as sommerfeld radiation boundary condition (Orlanski, 1976).

$$\frac{\partial P}{\partial n} = -\frac{1}{c} \frac{\partial P}{\partial t} \quad (33)$$

Reservoir free surface (S4) – At the free surface, surface waves are neglected which can be represented as:

$$P(x, y = H, t) = 0 \quad (34)$$

Finite Element Formulation

The finite element shape functions for the spatial variation of the fluid pressure P and structural displacement u are given by:

$$P = \{N\}^T \{P_e\}, \quad u = \{N'\}^T \{U_e\} \quad (35)$$

where

- $\{P_e\}$ = nodal pressure vector
 $\{U_e\}$ = nodal structural displacement vector
 $\{N\}$ = element shape function for pressure
 $\{N'\}$ = element shape function for displacement

Discretized Fluid Equation

The discretized wave equation at the fluid structure interface is given by:

$$[M_e^P]\{\ddot{P}_e\} + [C_e^P]\{\dot{P}_e\} + [K_e^P]\{P_e\} + \rho_w[R_e]^T\{\ddot{U}_e\} + \rho_w[R_e]^T[I]\ddot{u}_g = \{0\} \quad (36)$$

where

$$\begin{aligned}
 [M_e^P] &= \frac{1}{c^2} \int \{N\}^T \{N\} d\Omega && \text{fluid mass matrix} \\
 [K_e^P] &= \int \{\nabla N\}^T \{\nabla N\} d\Omega && \text{fluid stiffness matrix} \\
 [C_e^P] &= \frac{1}{c} \int \{N\}^T \{N\} d\Gamma && \text{fluid damping matrix} \\
 \rho_w[R_e] &= \rho_w \int \{n\}^T \{N\} \{N'\}^T d\Omega && \text{coupling mass matrix}
 \end{aligned}$$

Discretized Structure Equation

The equation of motion for the structure at the element level is given by:

$$[M_e]\{\ddot{U}_e\} + [C_e]\{\dot{U}_e\} + [K_e]\{U_e\} = -[M_e]\{\Gamma\}\ddot{u}_g + [R_e]\{P_e\} \quad (37)$$

where $\{\Gamma\}$ is an influence vector which transmits the support acceleration \ddot{u}_g to structural degrees of freedom and $[R_e]\{P_e\}$ represents the nodal force vector associated with the hydrodynamic pressure caused by the fluid.

Discretized Fluid-Structure Coupling Equation

The complete finite element discretized equations for the fluid-structure interaction problem are expressed as:

$$\begin{bmatrix} [M_e] & [0] \\ [M^{fs}] & [M_e^P] \end{bmatrix} \begin{Bmatrix} \{\ddot{U}_e\} \\ \{\ddot{P}_e\} \end{Bmatrix} + \begin{bmatrix} [C_e] & [0] \\ [0] & [C_e^P] \end{bmatrix} \begin{Bmatrix} \{\dot{U}_e\} \\ \{\dot{P}_e\} \end{Bmatrix} + \begin{bmatrix} [K_e] & [K^{fs}] \\ [0] & [K_e^P] \end{bmatrix} \begin{Bmatrix} \{U_e\} \\ \{P_e\} \end{Bmatrix} = \begin{Bmatrix} -[M_e]\{\Gamma\}\ddot{u}_g \\ -\rho_w[R_e]^T\{\Gamma\}\ddot{u}_g \end{Bmatrix} \quad (38)$$

where

$$[M^{fs}] = \rho_w[R_e]^T \text{ and } [K^{fs}] = -[R_e] \quad (39)$$

Coupling Matrix $[R_e]$ transforms both the structure acceleration and the support acceleration to pressure flux and also transforms hydrodynamic pressure into applied loads to the structure (ANSYS, R16.2).

4.2 Modeling of Floodwall and Reservoir System

In this study, two-dimensional 4-noded structural solid and 4-noded acoustic fluid elements are used to discretize the solid floodwall and reservoir water, respectively (ANSYS, R16.2). The floodwall is assumed to be linearly elastic and in a state of plane stress. The reservoir is assumed to be of uniform shape and water is considered as a compressible and inviscid fluid. The foundation of the floodwall reservoir system is assumed to be rigid. The length of the reservoir is chosen as two times the floodwall height (Zeydan, 2013) and the surface waves are neglected. Impedance loading condition which relates to the incident and reflected waves at the S3 boundary is used for absorbing the waves.

The two-dimensional finite element model of the floodwall reservoir system is shown in Fig. 9. The concrete is assumed to be homogeneous and isotropic with elasticity modulus of

22400 MPa, poisson's ratio of 0.20, and density of 2480 kg m^{-3} . The density and velocity of pressure wave in water are taken as 1000 kg m^{-3} and 1440 m/s respectively.

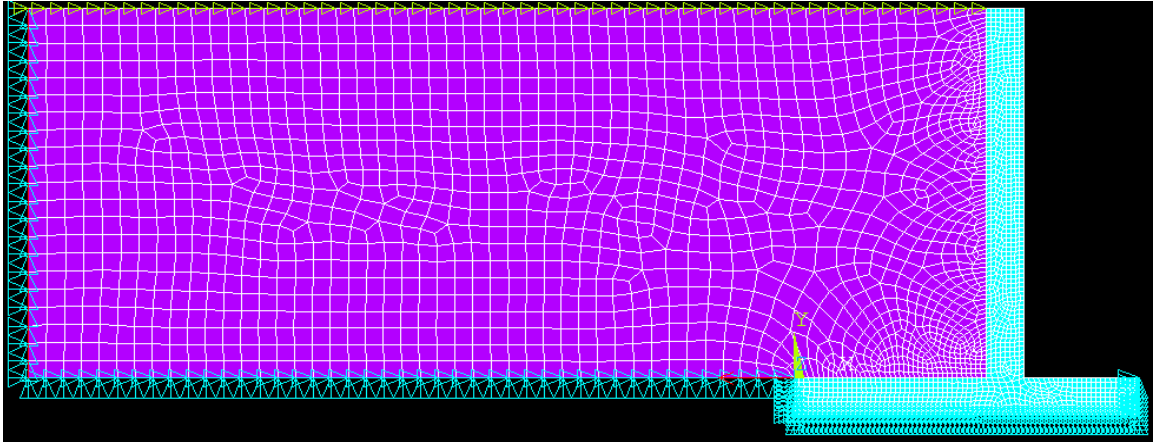


Fig. 17. Finite element model of floodwall reservoir system

4.3 Time History Analysis of Reservoir-Floodwall System

The linear transient dynamic analysis for the concrete floodwall is performed using direct integration method. In this model, Rayleigh damping is used for the dynamic analysis. Therefore, modal analysis of the FE model is carried out to calculate the Rayleigh damping coefficients. In this study for the modal analysis, damped mode-extraction method is used. This method is employed as it accounts for the damping due to impedance boundary condition at S3 and unsymmetrical mass and stiffness matrices due to the fluid structure interaction. Complex eigenvalues are obtained from the damped modal analysis. The real part of the eigenvalue physically represents the stability of the system and the imaginary part of the eigenvalue represents the natural frequency of the system. The first three natural frequencies of the reservoir-floodwall system are 6.37 Hz., 36.87 Hz., and 85.54 Hz. Clearly, the response of the floodwall for the seismic motion is primarily from the first two modes. Therefore, damping ratio of 5% are chosen for the first and the second vibration modes.

A time step of 0.005 seconds is chosen for the unconditionally stable implicit time marching scheme. The response of the floodwall is evaluated for 1975 Oroville earthquake scaled to 0.1g PGA (Fig. 10) and the time history of horizontal displacement at the wall crest is plotted as shown in Fig. 11. The maximum displacement (Δ_D) obtained from the displacement time history at wall crest is used for calculating fragility due to the excessive deformation failure mode. The hydrodynamic pressure envelope acting on the upstream face of the floodwall is shown in Fig. 12. This pressure envelope is very similar to what is observed in prior studies for concrete dams (Antunes and Carvalho, 2011).

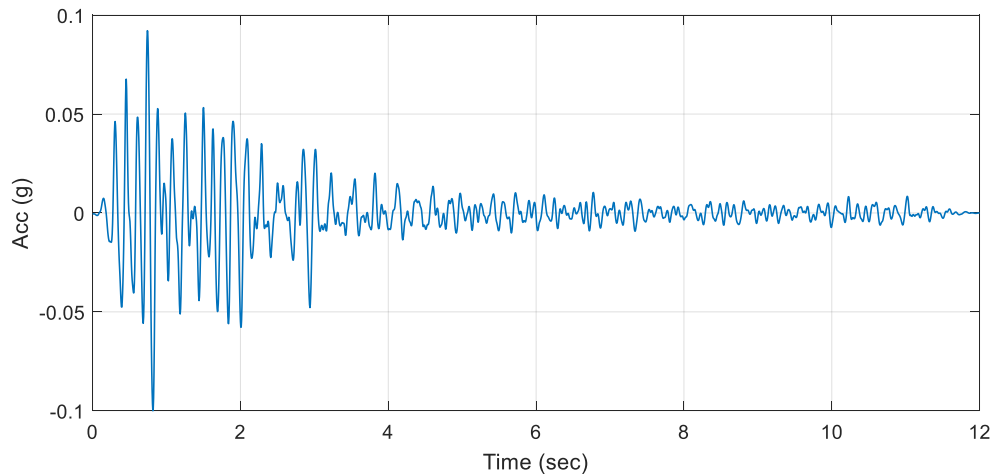


Fig. 18. Acceleration Time History of Oroville earthquake scaled to 0.1g PGA

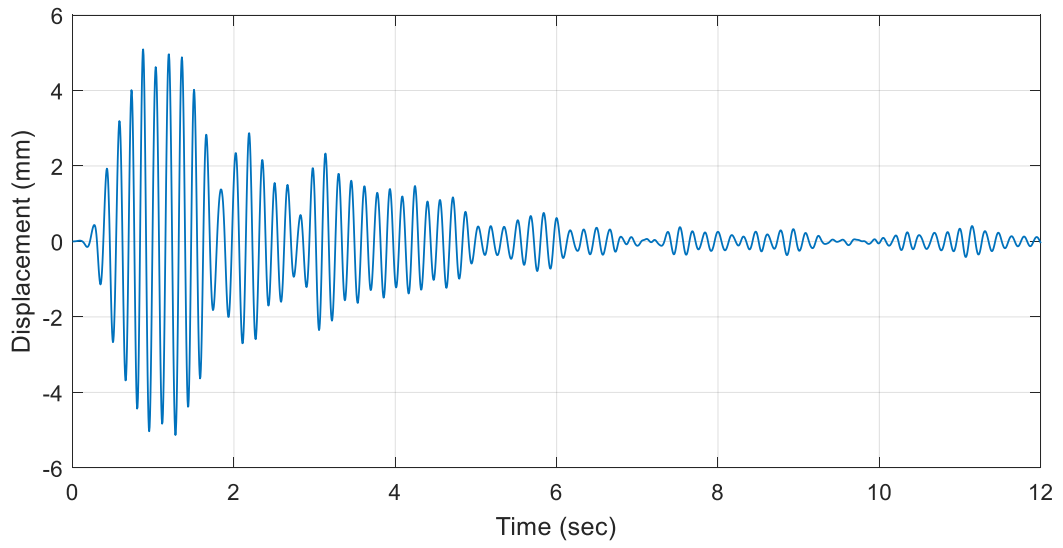


Fig. 19. Horizontal displacement time history at the wall crest with full reservoir

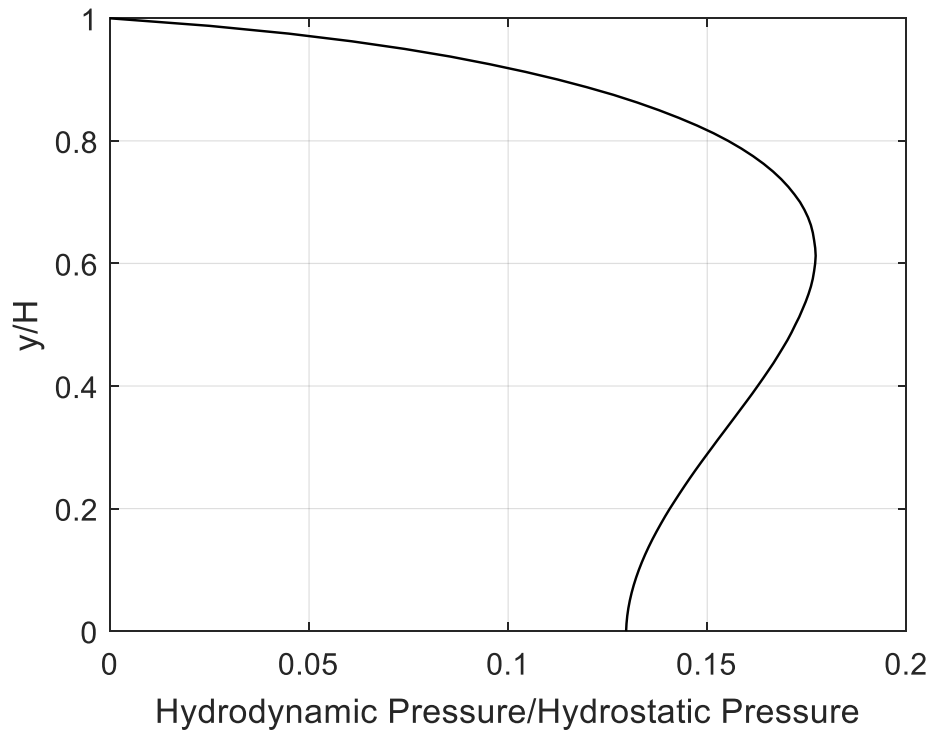


Fig. 20. Hydrodynamic Pressure envelope acting on the upstream face of the floodwall

4.4 Seismic Fragility Surface

Seismic fragility curves for the floodwall are evaluated by considering 10 recorded time histories as shown in Table 4. The response spectra of the ten ground motions scaled to 1g are shown in Fig. 13 for a damping ratio of 5%. Many of these spectra have peaks in the range of 6-7 Hz. and the first mode of the floodwall is 6.37 Hz. But some of these spectra also have peaks in the high frequency region and it can excite the second mode of the floodwall. Therefore, this fragility analysis can capture the effect of both low and high frequency modes.

Each ground motion is scaled to yield PGA values ranging from 0.1g to 0.8 g as an input for the floodwall model. A total of 10 finite element simulations are carried out for each PGA with a reservoir level of 2.5 m. The fragility analysis is carried out for material properties described in section 4.2 and the uncertainty is considered only in the seismic ground motions. Structural performance is evaluated with respect to the excessive deformation failure mode given by:

$$Z_{\Delta} = \Delta_c - \Delta_D \quad (40)$$

where, Δ_D = maximum crest displacement and $\Delta_c = 0.05\%$ of height of the floodwall (Tekie and Ellingwood, 2003)

The conditional probability of excessive deformation failure given peak ground acceleration (PGA) is expressed as:

$$P_f(\text{excessive deformation} | \text{PGA}) = P(Z_{\Delta} < 0) \quad (41)$$

The fitted fragility function is plotted from the simulation data using maximum likelihood estimation as shown in Fig. 14. Seismic fragility curves are generated for different reservoir levels ranging from 0 to 5m. These fragility curves can be combined and represent in

form of a seismic fragility surface as shown in Fig. 15. However, the purpose of seismic fragility surface is to utilize the surface plot in conjunction with flooding analysis and develop a fragility surface for the multi-hazard scenario. Combined multi-hazard fragility surface is presented in next section.

Table 16. Selected ground motions

Location	Station
Parkfield, 1966	Cholame - Shandon Array #12
San Fernando, 1971	Lake Hughes #12
Oroville-01, 1975	Oroville Seismograph Station
Friuli Italy-01, 1976	Tolmezzo
Gazli USSR, 1976	Karakyr
Tabas Iran, 1978	Dayhook
Norcia Italy, 1979	Cascia
Nahanni Canada, 1985	Site 2
Nahanni Canada, 1985	Site 3
Baja California, 1987	Cerro Prieto

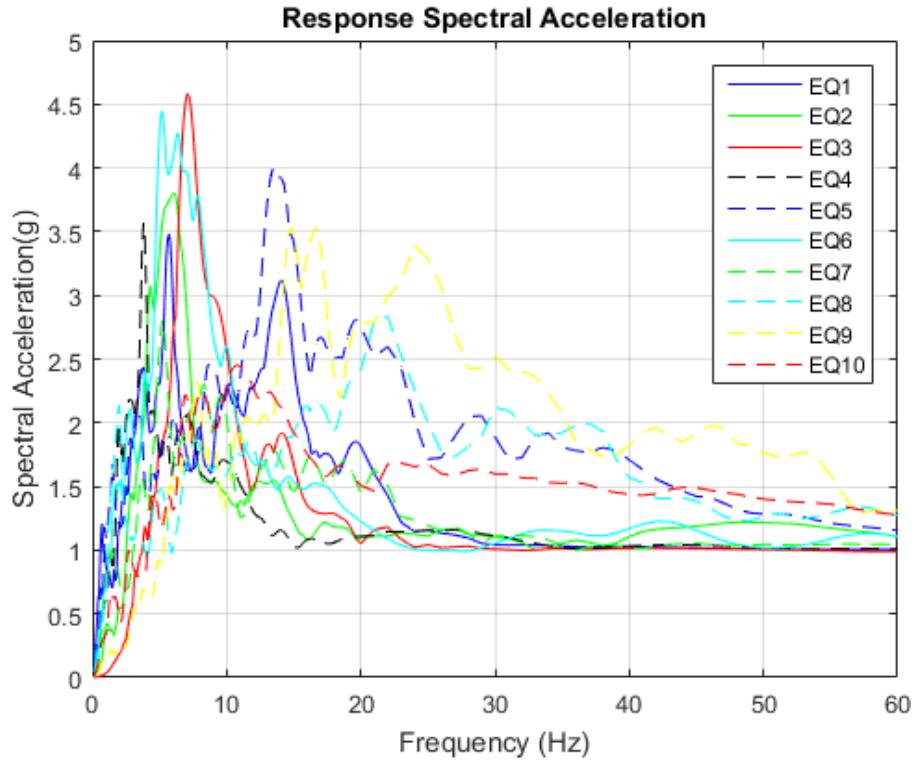


Fig. 21. Response spectral acceleration of selected ground motions

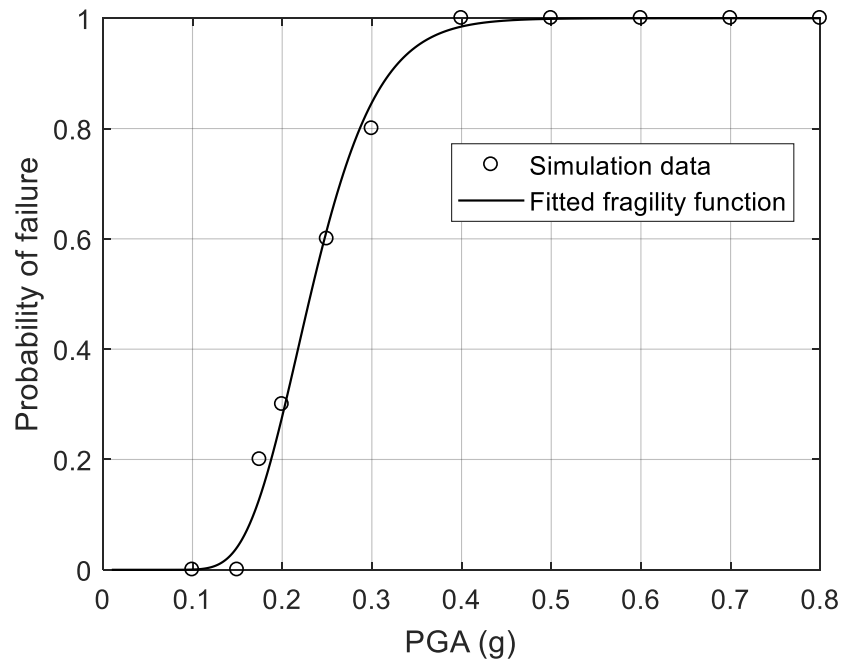


Fig. 22. Fragility curve due to excessive deformation failure mode for a flood level of 2.5 m

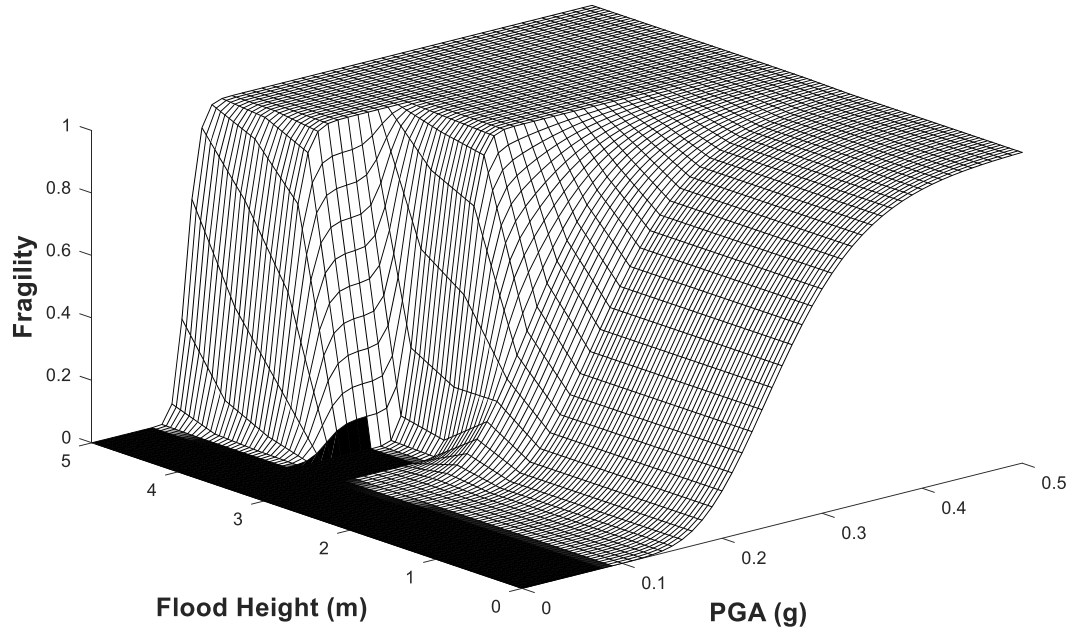


Fig. 23. Seismic fragility surface due to excessive deformation failure mode

5. Multi-hazard Fragility Assessment

A multi-hazard analysis is essential for determining the overall risk of the floodwall against all possible hazards. The probability of failure due to multiple hazards is evaluated by appropriately combining the probabilities of failure due to each hazard. Multi-hazard fragility surface (Fig. 16) is obtained by combining the seismic fragility surface (Fig. 15) and the system level flooding fragility curve (Fig. 7) using the following expression.

$$P(\text{system}) = \bigcup_i P(\text{system}_i | \text{hazard}) \quad (42)$$

where, $P(\text{system}_i | \text{hazard})$ is the system fragility of i^{th} hazard.

The floodwall can fail due to flooding hazard even without any seismic load. For lower magnitudes of flood height, the seismic hazard takes over the flooding hazard. However, the floodwall doesn't fail in seismic until it reaches a certain magnitude of PGA.

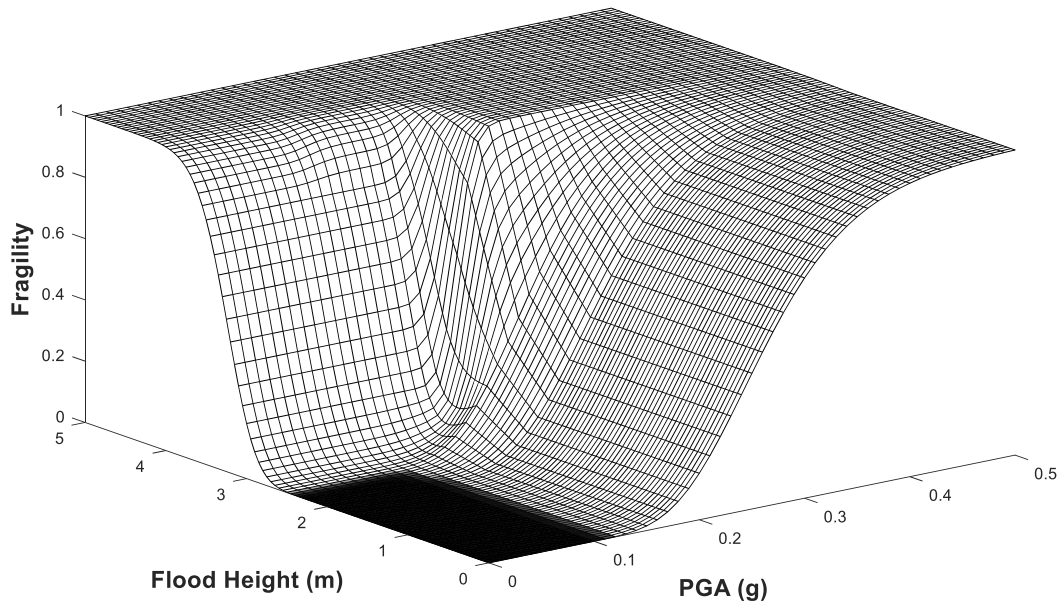


Fig. 24. Multi-hazard fragility surface

6. Conclusions

The conclusions related to the fragility of a concrete floodwall considering various comprehensive set of failure modes under a multi-hazard scenario of flooding and seismic events are:

- There is no failure in overturning of the floodwall and compression failure of concrete at the toe of the floodwall.

- For class 2 soil, the flooding fragility curves due to sliding of the floodwall and compression failure of foundation at the toe are almost zero for the functional height (around 4 m) of upstream water level.
- For the system level flooding fragility, the relative contribution of rupture failure mode is higher than other failure modes.
- The seismic fragility of a concrete floodwall is highly dependent upon the fluid-structure interaction.
- The seismic fragilities obtained for excessive deformation failure mode of the floodwall fit quite well with the cumulative lognormal distribution. The results indicate a median seismic fragility of 0.23g with a standard deviation of 0.25.
- For different heights of reservoir level seismic fragility curve changes to a fragility surface.
- From the multi-hazard fragility surface, the probability of system failure can be obtained for the corresponding flood height and peak ground acceleration.

REFERENCES

- Akhaveissy, A. H., and Malekshahi, M. (2012). "Transient Analysis of Dam-Reservoir Interaction," IACSIT Coimbatore Conferences IPCSIT, 28.
- ANSYS (R16.2) Mechanical APDL Theory Reference.
- Antunes, D. C. J. S., and Carvalho, M. R. F. (2011). "Large dam-reservoir systems: Guidelines and tools to estimate loads resulting from natural hazards," *Natural Hazards*, 59 (1), 75- 106.
- ASTM D2487-00. (2000). "Standard Classification of Soils for Engineering Purposes (Unified Soil Classification System)," ASTM International, West Conshohocken, PA.
- Bodda, S., Sandhu, H., and Gupta, A. (2016). "Fragility of a Flood Defense Structure Subjected to Multi-Hazard Scenario," ASME. International Conference on Nuclear Engineering.
- FEMA P-259. (2012). "Engineering Principles and Practices of Retrofitting Floodprone Residential Structures, Third Edition."
- Fenves, G., and Chopra, A.K. (1983). "Effects of reservoir bottom absorption on earthquake of concrete gravity dams," *Earthquake Engineering and Structural Dynamics*, 11, 809-829.
- Ju, B. S., and Jung, W. (2015). "Evaluation of Seismic Fragility of Weir Structures in South Korea," *Mathematical Problems in Engineering*, 10 pages.
- Kaida, H., Miyagawa, Y., and Kihara, N. (2016). "Methodology for Fragility Evaluation of a Seawall Against Tsunami Effects," ASME, International Conference on Nuclear Engineering.

- Khosravi, S., and Heydari, M. M. (2013). "Modelling of Concrete Gravity Dam Including Dam-Water-Foundation Rock Interaction," *World Applied Sciences Journal*, 22(4), 538-546.
- Lupoi, A. and Callari, C. (2011). "A probabilistic method for the seismic assessment of existing concrete gravity dams," *Structure and Infrastructure Engineering*, 8(10), 985-998.
- Orlanski, I. (1976). "A simple boundary condition for unbounded hyperbolic flows," *Journal of Computational Physics*, 21, 251-269.
- Perkins, R. H., Bensi, M. T., Philip, J., and Sancakatar, S. (2011). "Screening Analysis Report for the Proposed Generic Issue on Flooding of Nuclear Power Plant Sites Following Upstream Dam Failures," NRC, Washington, DC. US Nuclear Regulatory Commission, Office of Nuclear Regulatory Research, Division of Risk Analysis.
- Rajabalinejad, M., Van Gelder, P. H. A. J. M., and Vrijling, J. K. (2008). "Probabilistic Finite Elements With Dynamic Limit Bounds; A Case Study: 17th Street Flood Wall, New Orleans," *International Conference on Case Histories in Geotechnical Engineering*. 43.
- Sandhu, H. K. (2015). "Flooding Fragility of Concrete Gravity Dam-Foundation System," Master of Science Thesis, Department of Civil Engineering, North Carolina State University, Raleigh, NC.
- Tekie, P. B. and Ellingwood, B. R. (2003). "Seismic fragility assessment of concrete gravity dams," *Earthquake Engineering and Structural Dynamics*, 32(14), 2221-2240.
- Terzaghi, K. (1943). *Theoretical Soil Mechanics*. John Wiley and Sons, New York.

Zeydan, B. A. (2013). "Hydrodynamic Analysis of Concrete Gravity Dams Subjected to Ground motion," 9th Symposium of ICOLD European Club.

PART IV: SUMMARY AND CONCLUSIONS

1. Summary

The system level fragility of a flood defense structure, built to protect critical and toxic facilities has gained significant importance in the recent years. In this research, various failure modes are considered to evaluate fragilities for failure of a flood defense structure under a multi-hazard scenario. In the first part, the research analyzes the effect of scouring on the foundation failure of a concrete weir structure due to rupture. The effect of scouring in the rupture analysis is included by varying the scour width and the scour depth. This research incorporates uncertainties in permeability ratio, specific gravity and porosity of soil. The challenges associated with the accuracy and efficiency of the finite element model for the rupture analysis is also analyzed.

The second part of this research focuses on the multi-hazard assessment of a concrete floodwall. Finite element analysis is used for modeling the seismic behavior as well as the seepage through the foundation. Uncertainties in several random variables that characterizes the material properties, foundation soil, flooding and seismic loads are employed using the Monte Carlo simulation. Multi-hazard fragility surface is obtained by combining the seismic fragility surface and the system level flooding fragility curve.

2. Conclusions

The primary observations and the key conclusions of this research are summarized as follows:

- For the seepage flow under a concrete flood defense structure, the finite element model with either 6-noded triangular or 8-noded quadrilateral elements exhibits smaller error compared to conventional 4-noded quadrilateral elements for the same element size.

Use of adaptive mesh refinement technique reduces the analysis computation cost which is important for a probabilistic study to evaluate the rupture fragility.

- If the size of the elastic half space is less than an optimal size, then the exit gradient results can be either underestimated or overestimated. Based on the convergence study, the dimensions of the elastic half space should be at least 2.5 times more than the width of the concrete flood defense structure.
- The scour profile has a significant effect on the fragility curves. For a constant flood height and scour depth, the probability of rupture failure increases with decrease in the scour width.
- The system level fragility curve for flooding is obtained by considering the various failure modes of the floodwall. The probabilities of failure at different flood heights is governed by different failure modes. The relative contribution of rupture failure mode is higher than other failure modes.
- The seismic fragility of a concrete floodwall is highly dependent upon the fluid-structure interaction. A higher level of reservoir results in greater hydrodynamic pressure leading to greater chances of failure.

3. Recommendations for Future Research

It is recommended that future studies might consider evaluating the total risk of failure for the flood defense structure. The total risk is evaluated by convolution of the hazard and the fragility curve. The combined risk due to multiple hazards can be obtained by using total probability theorem:

$$P(R) = \sum_i P(R|H_i)P(H_i) \quad (1)$$

where: $P(R)$ is the total risk, $P(R|H_i)$ is the conditional probability of failure, and $P(H_i)$ is the i^{th} hazard.

It is suggested that further research should consider the following aspects:

- Ground motions chosen for the seismic fragility analysis should be consistent with the probabilistic seismic hazard analysis (PSHA) requirements for the site location. The number of ground motions can be increased to obtain better results.
- Seismic fragility curves for other failure modes should be considered. The effect of soil-structure interaction on seismic fragility needs to be evaluated.
- Finally, the foundation model should comprise of non-uniform soils.